UNIVERSITÀ DEGLI STUDI DI GENOVA
SCUOLA DI SCIENZE MEDICHE E FARMACEUTICHE

CORSO DI LAUREA MAGISTRALE IN MEDICINA E CHIRURGIA

ANNO ACCADEMICO 2025/2026

TESI DI LAUREA

Added Diagnostic Value of High-Resolution 3D MRI Sequences in the Early Diagnosis of Spinal Metastases in Pediatric CNS Tumors

RELATORE

Prof. Andrea Rossi

CANDIDATO

Giovanni Celle

CORRELATORE

Dott.ssa Antonia Ramaglia

Table of Contents

List of Abbreviations

Abbreviation	Full Term
BBB	Blood-Brain Barrier
bFFE	balanced Fast-Field Echo
bSSFP	balanced Steady-State Free Precession
CISS	Constructive Interference in Steady State
CNS	Central Nervous System
CP	Craniopharyngioma
CPS	Cancer Predisposition Syndrome
CSF	Cerebrospinal Fluid
CT	Computed Tomography
DE-SE	Driven Equilibrium Spin Echo
DIPG	Diffuse Intrinsic Pontine Glioma
DRIVE	Driven Equilibrium
EP	Ependymoma
FIESTA	Fast Imaging Employing Steady-State Acquisition
FOV	Field Of View
HGG	High-Grade Glioma
MB	Medulloblastoma
MRI	Magnetic Resonance Imaging
PV	Pathological Variant
RANO	Response Assessment in Neuro-Oncology
RAPNO	Response Assessment in Pediatric Neuro-Oncology
SE	Spin echo
SNR	Signal-to-Noise Ratio
T1WI	T1-weighted imaging
WBRT	Whole-Brain Radiotherapy

1 Introduction

1.1 Pediatric Central Nervous System (CNS) Tumors

1.1.1 Definition and WHO classification

Central nervous system (CNS) tumors comprise a heterogeneous group of neoplastic diseases arising within the brain, spinal cord, meninges, cranial and spinal nerves, or related structures. According to the fifth edition of the WHO Classification of Tumours of the Central Nervous System, published in 2021, CNS tumors include more than one hundred distinct entities and subtypes, each characterized by specific histological, molecular, clinical, therapeutic, and prognostic features [1].

CNS tumors may arise primarily from neural, glial, meningeal, or other CNS-associated tissues, or may represent secondary involvement from extracranial malignancies. Although the distinction between benign and malignant tumors is commonly used, it is particularly complex in neuro-oncology. Histologically benign lesions may cause substantial morbidity, or even life-threatening complications, when located near eloquent or critical structures, whereas some histologically aggressive tumors may show variable behavior depending on their molecular profile, location, and available treatment options.

Tumor grading in the CNS has historically differed from grading systems used for non-CNS neoplasms. Traditionally, grades were assigned mainly on the basis of histopathological features and expected clinical behavior. In this framework, different tumor entities could share the same grade despite substantial biological differences, because grading was intended to reflect an idealized estimate of aggressiveness and survival.

The fifth edition of the WHO classification introduced important changes to CNS tumor grading, aligning it more closely with grading principles used in other organ systems while preserving features specific to neuro-oncology. In particular, grading is now applied within individual tumor types rather than across biologically distinct entities. This approach allows a more precise correlation between tumor type, molecular profile, and clinical behavior,

while acknowledging that prognosis is increasingly influenced by advances in molecular diagnostics and targeted therapies [1].

A further major innovation of the 2021 WHO classification was the formal recognition of pediatric-
type CNS tumor entities, distinct from adult-type tumors. This distinction reflects the growing evidence that many pediatric CNS tumors differ substantially from their adult counterparts in terms of molecular alterations, anatomical distribution, clinical course, and therapeutic response [1,2].
Molecular alterations have progressively become central to the classification of CNS tumors. They were first systematically incorporated into diagnostic criteria in the 2016 WHO classification and were subsequently refined through the work of the Consortium to Inform Molecular and Practical Approaches to CNS Tumor Taxonomy — cIMPACT-NOW — which provided interim updates between WHO editions [3].

The integration of molecular data has promoted a layered diagnostic approach, particularly useful for entities in which histomorphological and immunohistochemical features alone may be insufficient for accurate classification. Molecular characterization also provides relevant prognostic and therapeutic information and has significantly improved the understanding of CNS tumor biology and clinical management [4].
In line with this evolution, the cIMPACT-NOW committee proposed in 2025 that unique DNA- or RNA-based genetic alterations should be considered among the defining criteria for the establishment of new CNS tumor types and subtypes [5].

1.1.2 Epidemiology: Incidence and Mortality

In adults, primary central nervous system tumors account for a relatively small proportion of all neoplasms. In this age group, intracranial tumors are more frequently secondary to metastatic spread from systemic malignancies than primary CNS neoplasms. Several studies have reported that brain metastases are at least as common as, and in some series up to ten times more frequent than, primary brain tumors. Lung cancer, breast cancer, and melanoma account for a substantial proportion of brain metastases, and metastatic CNS involvement is

consistently associated with increased morbidity and mortality, regardless of the primary tumor type [6].

In the pediatric population, conventionally defined as individuals aged 0–19 years, primary CNS tumors have a markedly different epidemiological profile. They represent the most common solid tumors of childhood and rank among the leading pediatric cancers. According to the Central Brain Tumor Registry of the United States (CBTRUS), the overall incidence of CNS tumors in children and adolescents was 6.23 per 100,000 population, while the incidence of malignant CNS tumors was 3.55 per 100,000 population. These estimates were based on data collected between 2014 and 2018 and covered approximately 98% of the United States population [7].

Primary CNS tumors are also a major cause of cancer-related mortality in children and adolescents. According to the same epidemiological data, they account for an average mortality rate of 0.66 deaths per 100,000 population. CNS tumors represent the leading cause of cancer-related death in children aged 5–14 years and the second leading cause in children aged 0–4 years and adolescents aged 15–19 years, after leukemia [8].

The epidemiology of CNS tumors also varies across age groups. In young adults, aged 20–39 years, brain and other CNS tumors remain relatively frequent compared with the general population, with reported incidence rates of 3.25 per 100,000 for malignant tumors and 8.71 per 100,000 for non-malignant tumors [9].

Histopathological distribution differs substantially between pediatric patients and adults. In children and adolescents, the most frequently encountered entities include pilocytic astrocytoma and tumors of the sellar region, including pituitary tumors. In infants younger than one year of age, gliomas and embryonal tumors, particularly atypical teratoid/rhabdoid tumors, are among the most common diagnoses.

1.1.3 Pathogenesis and Risk Factors

The pathogenesis of CNS tumors is complex and involves the accumulation of genetic and epigenetic alterations affecting neural stem cells, progenitor cells, or lineage-committed cells

within the central nervous system. These alterations may disrupt key regulatory pathways controlling cell proliferation, differentiation, DNA repair, and apoptosis. In line with this biological complexity, the 2021 WHO classification places increasing emphasis on the identification of molecular alterations for diagnostic classification, prognostic stratification, and therapeutic decision-making [1].

Ionizing radiation is one of the best-established environmental risk factors for the development of CNS tumors. This association has been documented in patients previously exposed to therapeutic cranial irradiation, as well as in studies evaluating environmental and occupational exposure [10]. Exposure to ionizing radiation from diagnostic procedures during pregnancy, including computed tomography and nuclear medicine examinations, has also raised concerns regarding potential long-term cancer risk in offspring, although this risk depends on dose, gestational age, and the specific imaging modality used [11].

In pediatric patients, CNS tumors are also among the neoplasms most frequently associated with cancer predisposition syndromes (CPS). The best-known syndromes include neurofibromatosis type 1 and type 2. Neurofibromatosis type 1 is associated with an increased risk of low-grade gliomas, particularly optic pathway gliomas, whereas neurofibromatosis type 2 is classically associated with vestibular schwannomas, meningiomas, and ependymomas. Li-Fraumeni syndrome, caused by germline TP53 pathogenic variants, is associated with a broad spectrum of CNS tumors, including medulloblastoma, astrocytoma, glioblastoma, and choroid plexus carcinoma.

Advances in molecular diagnostics and the increasing use of next-generation sequencing have led to the recognition of several previously underdiagnosed germline pathogenic variants associated with pediatric CNS tumors. This has improved the identification of patients with inherited cancer predisposition and has important implications for genetic counseling, surveillance, and treatment planning.

For example, a proportion of patients with WNT-activated medulloblastoma harbor germline loss-of-function pathogenic variants in the APC tumor suppressor gene, leading to the diagnosis of familial adenomatous polyposis. Similarly, among pediatric patients with SHH-

activated medulloblastoma, germline pathogenic variants in PTCH1 or SUFU may be associated with nevoid basal cell carcinoma syndrome, historically known as Gorlin syndrome [12].

1.2 Clinical Presentation

1.2.1 Signs and Symptoms of CNS Neoplasm

Headache is one of the most common presenting symptoms of intracranial CNS tumors in children. It is often related to increased intracranial pressure, mass effect, or obstruction of cerebrospinal fluid pathways. Tumor-related headache may be more prominent during the night or upon awakening, particularly when associated with vomiting or other signs of raised intracranial pressure.

Vomiting is another frequent symptom, especially in tumors causing hydrocephalus or involving the posterior fossa and brainstem. It is commonly associated with increased intracranial pressure, although it may also occur in the absence of overt pressure elevation when tumors involve structures related to emetic control, such as the area postrema or the nucleus tractus solitarius.

Seizures may occur in patients with CNS tumors, although their frequency varies widely according to tumor type, growth rate, cortical involvement, and anatomical location. They are more commonly associated with slow-growing, low-grade, supratentorial tumors. Lesions involving the frontal, temporal, and parietal cortices are particularly associated with epileptogenesis, whereas infratentorial tumors are less commonly associated with seizures. Although seizures are not the most frequent presenting symptom in pediatric CNS tumors, they may significantly affect morbidity, mortality, and quality of life [13].

Focal neurological deficits include a wide range of clinical manifestations depending on the anatomical structures involved. These may include motor weakness, ataxia, cranial nerve palsies, visual disturbances, aphasia, behavioral changes, cognitive impairment, and memory deficits. In children, these symptoms may be subtle, progressive, or difficult to recognize, particularly in younger age groups.

Increased intracranial pressure is an important clinical sign that may suggest the presence of a space-occupying intracranial lesion. It may result from tumor mass effect, peritumoral edema, obstruction of cerebrospinal fluid circulation, or hydrocephalus. Clinical manifestations include headache, vomiting, papilledema, altered consciousness, and, in severe cases, signs of brain herniation. Neuroimaging with computed tomography or magnetic resonance imaging is essential to identify ventricular enlargement, mass effect, herniation, and the underlying tumor.

Pediatric patients, especially infants and young children, often present with nonspecific symptoms. A meta-analysis including 74 studies and more than 4,000 children reported that the most common symptoms at diagnosis were headache, observed in 33% of cases, and vomiting, observed in 32%. These were followed by motor abnormalities, including gait and coordination disturbances, in 27% of cases, papilledema in 13%, and seizures in 13% [14]. The same study also highlighted that specific combinations of symptoms may suggest particular tumor locations. In children, CNS tumors most frequently involve the infratentorial compartment, reported in 45–60% of cases, followed by the cerebral hemispheres in 25–40% and midline supratentorial structures in 15–20% [14].

1.3 Metastases and Leptomeningeal Spread

Intracranial metastases may occur in patients with primary extracranial malignancies either at initial diagnosis, in which case they are defined as synchronous brain metastases, or later during the course of disease. CNS metastatic involvement has major clinical implications, as it may cause neurological symptoms, reduce quality of life, and significantly affect prognosis. From a therapeutic perspective, the blood–brain barrier may limit the efficacy of systemic treatments, often requiring local approaches such as brain-directed radiotherapy or neurosurgical resection [6].

The incidence of brain metastases varies according to primary tumor type, molecular subtype, and disease stage. In adults, lung cancer, breast cancer, and melanoma represent the most common sources of brain metastases. Non-small cell lung cancer accounts for a large

proportion of cases because of its high prevalence, whereas small cell lung cancer is characterized by a particularly high propensity for CNS dissemination. Prognosis remains poor in patients presenting with brain metastases at diagnosis, with population-based estimates varying according to primary tumor type, age, performance status, and extent of systemic disease [15]. Because of the frequency and prognostic impact of CNS involvement, screening neuroimaging at diagnosis is recommended in selected tumor types and stages, according to current clinical guidelines [6].

Leptomeningeal metastasis, also referred to as leptomeningeal carcinomatosis, occurs when neoplastic cells infiltrate the leptomeninges of the brain and spinal cord and disseminate within the cerebrospinal fluid (CSF). Tumor cells may reach the leptomeningeal compartment through hematogenous spread, direct extension from intra-axial brain or spinal tumors, perineural or endoneural routes, or, in selected cases, iatrogenic seeding after surgical procedures [16]. Once tumor cells enter the CSF spaces, they may disseminate along the meningeal surfaces following CSF circulation and gravitational pathways. This mechanism is particularly relevant for primary CNS tumors with a tendency toward leptomeningeal seeding, in which spinal “drop metastases” may develop along the surface of the spinal cord, cauda equina nerve roots, and dural cul-de-sac.

Leptomeningeal metastatic disease is associated with a poor prognosis and substantial neurological morbidity. In systemic malignancies, reported median survival remains limited, often ranging from 1 to 4 months despite site-specific therapeutic strategies [17]. In pediatric primary CNS tumors, early recognition of leptomeningeal and spinal dissemination is therefore essential for staging, risk stratification, treatment planning, and follow-up surveillance.

1.4 Spinal metastases in pediatric patients

Spinal tumors are less common than intracranial tumors in children, but their diagnosis and management are often complex and require a multidisciplinary approach. Lesions involving the spinal canal are commonly classified according to their anatomical compartment as extradural, intradural extramedullary, or intramedullary.

Extradural lesions usually arise from the vertebral column or epidural space and may include benign entities, such as vertebral hemangiomas, as well as aggressive or metastatic lesions capable of causing vertebral collapse and spinal cord compression. Intradural lesions are further divided into extramedullary and intramedullary tumors. Intradural extramedullary tumors arise outside the spinal cord but within the dural sac, whereas intramedullary tumors originate within the spinal cord parenchyma. Although many primary intradural tumors may be histologically low grade, they can still cause significant neurological morbidity due to compression or infiltration of neural structures.

In the context of pediatric primary CNS tumors, spinal metastatic disease most commonly reflects leptomeningeal dissemination through the cerebrospinal fluid. The term “drop metastases” refers to tumor deposits that seed the spinal subarachnoid spaces after dissemination from a primary intracranial or spinal CNS tumor. On MRI, drop metastases typically appear as focal or multifocal intradural extramedullary deposits along the surface of the spinal cord, cauda equina nerve roots, or dural cul-de-sac. They may show nodular or linear enhancement after contrast administration, sometimes producing a diffuse “sugar-coating” pattern along the leptomeningeal surfaces. However, small, early, or poorly enhancing deposits may be difficult to identify on post-contrast T1-weighted sequences alone.

Because tumor cells can disseminate along CSF pathways and settle in dependent regions under the influence of CSF flow and gravity, spinal drop metastases are frequently encountered in caudal sites, particularly along the lumbosacral canal, cauda equina, and dural cul-de-sac. Accurate evaluation of these regions is therefore essential in pediatric CNS tumors with a known tendency toward leptomeningeal spread.

1.5 Diagnostic Imaging and Management

1.5.1 Computed Tomography (CT) vs. Magnetic Resonance Imaging (MRI)

The 2021 WHO classification of CNS tumors emphasizes the need for an integrated, layered diagnostic approach combining histopathological, molecular, and radiological information.

In this evolving framework, neuroimaging remains essential both at initial diagnosis and throughout follow-up. It contributes to lesion detection, anatomical localization, differential diagnosis, surgical planning, treatment response assessment, and surveillance for relapse or metastatic dissemination [1].

Computed tomography (CT) and magnetic resonance imaging (MRI) are the main imaging modalities used in the evaluation of CNS disease. CT is widely available, rapid, and particularly useful in emergency settings, especially for the detection of acute hemorrhage, hydrocephalus, calcifications, bone involvement, and mass effect. However, CT has limited soft-tissue contrast compared with MRI and exposes patients to ionizing radiation, an important limitation in children, who are more sensitive to radiation-related risks and may require repeated imaging examinations over time.

MRI is the imaging modality of choice for the evaluation of known or suspected CNS tumors. Its superior soft-tissue contrast, multiplanar capability, and wide range of tissue contrasts allow detailed assessment of tumor location, extension, internal structure, relationship with adjacent neurovascular structures, and associated complications. In pediatric neuro-oncology, MRI is therefore central not only for diagnosis, but also for staging, treatment planning, and longitudinal surveillance.

Contrast-enhanced MRI plays a key role in the assessment of blood–brain barrier disruption, tumor vascularity, residual disease, recurrence, and leptomeningeal dissemination. Gadolinium-based contrast agents shorten T1 relaxation time, producing signal hyperintensity on T1-weighted images in regions where contrast material accumulates. This mechanism is particularly useful for identifying enhancing tumor components and leptomeningeal deposits. However, reliance on contrast enhancement alone may be insufficient, especially in small, early, poorly enhancing, or non-enhancing lesions.

Despite its advantages, MRI also has limitations. It is less readily available than CT in some settings, requires longer acquisition times, and is more susceptible to motion artifacts. In younger children, sedation or general anesthesia may be necessary to obtain diagnostic-

quality images, adding logistical complexity and potential procedural risk. These limitations are particularly relevant in pediatric patients requiring repeated follow-up examinations.

For spinal assessment in pediatric CNS tumors, MRI is the reference imaging technique because it allows evaluation of the entire neuraxis without ionizing radiation. Conventional post-contrast T1-weighted sequences remain central for detecting enhancing leptomeningeal disease, but high-resolution heavily T2-weighted or myelographic sequences may provide additional diagnostic information by improving visualization of small intradural deposits, nerve roots, CSF spaces, and the dural cul-de-sac.

1.5.2 Conventional Protocols and RAPNO Guidelines

The Response Assessment in Pediatric Neuro-Oncology (RAPNO) working group is an international multidisciplinary initiative established to develop standardized imaging and response assessment criteria specifically tailored to pediatric CNS tumors. Since its creation, RAPNO has published consensus recommendations for several pediatric neuro-oncological entities, including medulloblastoma, ependymoma, high-grade glioma, low-grade glioma, and craniopharyngioma.

RAPNO criteria provide guidance on imaging acquisition, interpretation, and response assessment, with the aim of improving reproducibility across institutions and clinical trials. Standardization is particularly important in pediatric neuro-oncology, where differences between local and central imaging interpretations may affect the assessment of residual disease, metastatic dissemination, treatment response, and ultimately risk stratification. Previous studies have reported discordance rates of up to 25% between local and central neuroradiological review, underscoring the clinical relevance of standardized imaging criteria [18].

MRI is considered the reference imaging modality for diagnosis, staging, treatment planning, and follow-up of pediatric CNS tumors. Within this framework, RAPNO recommendations emphasize the value of high-quality MRI protocols, including three-dimensional sequences when appropriate. Three-dimensional acquisitions allow multiplanar reconstructions and volumetric assessment, improving the evaluation of small, irregularly shaped, or anatomically complex lesions compared with conventional two-dimensional imaging [19].

Nevertheless, MRI may not always be available as the first-line examination, particularly in emergency settings or in centers with limited access to pediatric MRI. In these circumstances, CT may be used for initial evaluation, especially when rapid assessment is required. However, CT has lower soft-tissue contrast than MRI and exposes children to ionizing radiation, which is a relevant limitation in patients who may require repeated imaging over time [20].

The need for pediatric-specific response criteria reflects important biological and imaging differences between pediatric and adult CNS tumors. For example, pediatric high-grade gliomas differ from adult high-grade gliomas in anatomical distribution, molecular profile, likelihood of leptomeningeal dissemination, and frequency of non-enhancing tumor components. Pediatric high-grade gliomas may appear as infiltrative lesions with heterogeneous contrast enhancement or may be largely non-enhancing. Therefore, assessment based exclusively on contrast enhancement may underestimate tumor extent. This is one of the reasons why RAPNO criteria incorporate non-enhancing disease, including areas of abnormal T2/FLAIR signal, into response assessment, differing from adult-oriented RANO criteria [21].

In the context of primary CNS tumors with a known risk of leptomeningeal dissemination, spinal MRI is an essential component of staging and follow-up. RAPNO recommendations suggest that brain and spine imaging should preferably be performed in a single session, in order to avoid repeated appointments, additional sedation, and multiple contrast agent administrations. Spinal MRI should include complete evaluation of the spinal canal, with adequate coverage of both upper and lower spinal segments, including the conus, cauda equina, and dural cul-de-sac.

Recommended spinal MRI protocols include post-contrast T1-weighted sequences, such as sagittal two-dimensional spin-echo acquisitions and axial or volumetric post-contrast sequences, depending on the institutional protocol. In addition, heavily T2-weighted myelographic sequences, including CISS, FIESTA, or DRIVE, are strongly recommended as complementary acquisitions. These sequences generate high contrast between

hyperintense cerebrospinal fluid and hypointense nerve roots or intradural tumor deposits, thereby improving the visualization of small, subtle, or non-enhancing lesions. They may also help distinguish true metastatic deposits from mimickers such as CSF pulsation artifacts, reducing the risk of false-positive interpretation.

These recommendations are particularly relevant for tumor entities with a recognized tendency toward leptomeningeal seeding, such as medulloblastoma, ependymoma, high-grade glioma, and diffuse intrinsic pontine glioma. Conversely, entities such as craniopharyngioma generally do not require routine spinal surveillance in the absence of specific clinical or radiological indications [19].

1.5.3 Current Treatment Modalities

The treatment of pediatric CNS tumors is multidisciplinary and may include neurosurgery, chemotherapy, radiotherapy, targeted therapies, or combinations of these approaches. Therapeutic planning depends on several factors, including tumor type, molecular profile, anatomical location, extent of disease, patient age, clinical condition, and presence of metastatic dissemination.

Surgery plays a central role in the management of many pediatric CNS tumors. Surgical procedures may be performed for diagnostic purposes, such as biopsy, or with therapeutic intent, including maximal safe resection, cytoreduction, or decompression. Surgery may also be required to manage complications such as hydrocephalus, for example through external ventricular drainage or cerebrospinal fluid diversion procedures. The feasibility and extent of resection depend largely on tumor location, relationship with eloquent neural structures, vascular anatomy, and expected surgical morbidity.

For posterior fossa tumors such as pilocytic astrocytoma and ependymoma, complete or near-complete resection is often an important therapeutic goal, although it may be limited by the risk of injury to cranial nerves, brainstem structures, and major vessels, particularly for lesions involving the cerebellopontine angle or ventral brainstem. By contrast, surgical management of brainstem tumors is more limited. Focal brainstem lesions may be approached surgically in selected cases, whereas diffuse intrinsic pontine glioma is generally

not amenable to resection. In these tumors, biopsy may be considered when imaging findings are atypical, when molecular characterization is required, or when enrollment in molecularly guided therapeutic protocols is planned [22].

The principle of maximal safe resection reflects the balance between oncological benefit and preservation of neurological function. Although residual tumor burden may be associated with poorer outcome in several tumor entities, aggressive resection must be weighed against the risk of permanent neurological morbidity when lesions are adjacent to or infiltrate critical structures [23,24].

Chemotherapy is widely used in pediatric neuro-oncology, either as adjuvant treatment after surgery, in combination with radiotherapy, or as part of treatment strategies aimed at delaying or reducing radiation exposure in younger children. Its efficacy depends on tumor biology, molecular subtype, drug sensitivity, and the ability of therapeutic agents to reach the central nervous system. The blood–brain barrier may limit the penetration of several systemic treatments, although its integrity varies according to tumor type, vascular permeability, and treatment-related changes [25].
Improving drug delivery to CNS tumors remains a major therapeutic challenge. Advances in molecular profiling have led to the development of targeted therapies and novel delivery strategies aimed at exploiting specific biological vulnerabilities of tumor cells and improving treatment response [26].

Radiation therapy is another cornerstone of treatment for several pediatric CNS tumors, including medulloblastoma, ependymoma, and selected gliomas. It may be used after surgery, in combination with chemotherapy, or as part of disease-control strategies in metastatic or recurrent disease. However, irradiation of the developing brain and spine is associated with relevant short- and long-term adverse effects, including neurocognitive impairment, endocrine dysfunction, vascular complications, hearing loss, growth disturbances, and secondary malignancies. These risks are particularly important in children, who are more vulnerable to radiation-related toxicity and may survive long enough to experience delayed complications [11,28,29]. For this reason, modern radiotherapy aims to optimize tumor control while minimizing dose to healthy tissues. Techniques such as

stereotactic radiotherapy and proton beam therapy allow more precise dose delivery and may reduce irradiation of uninvolved structures compared with conventional photon-based approaches. Proton beam therapy is particularly attractive in pediatric patients because of the physical properties of protons and the Bragg peak effect, which can reduce exit dose and lower integral dose to surrounding tissues. Nevertheless, the role and long-term benefit of these techniques continue to depend on tumor type, disease extent, availability, and the strength of clinical evidence [29].

In patients with leptomeningeal or spinal metastatic dissemination, treatment planning may require craniospinal irradiation, focal radiation boosts, systemic or intrathecal chemotherapy, and closer imaging surveillance. Therefore, accurate detection of spinal metastases is clinically relevant, as it may directly influence risk stratification, radiation fields, treatment intensity, and follow-up strategy.

1.6 The 3D DRIVE sequence

1.6.1 Technical Principles and Contrast Features

3D DRIVE, acronym for Driven Equilibrium, is a high-resolution, heavily T2-weighted, fluid-sensitive MRI sequence based on a three-dimensional turbo spin-echo acquisition combined with a driven equilibrium magnetization recovery module. Similar techniques are known under different vendor-specific names, including fast recovery fast spin-echo approaches. The sequence is designed to obtain high signal from fluids, such as cerebrospinal fluid, while maintaining high spatial resolution and allowing multiplanar reconstructions.

The physical principle underlying DRIVE is derived from the Driven Equilibrium Fourier Transform (DEFT) technique, first introduced in 1969 and initially applied in spectroscopy [30]. Subsequent developments demonstrated its usefulness in clinical imaging, particularly for tissues or fluids characterized by long T1 and T2 relaxation times, where the recovery of longitudinal magnetization can be exploited to improve acquisition efficiency and fluid signal [31]. From a technical perspective, the driven equilibrium module consists of an additional radiofrequency pulse applied at the end of the echo train. This pulse restores residual transverse magnetization to the longitudinal axis, thereby accelerating the apparent

recovery of longitudinal magnetization. As a result, shorter repetition times can be used while preserving a high signal-to-noise ratio and strong T2-weighted contrast from fluids [32].

These properties produce images in which hyperintense fluids, such as cerebrospinal fluid or synovial fluid, provide a natural high-contrast background against hypointense solid structures, including nerve roots, membranes, and small intradural lesions. Compared with conventional T2-weighted turbo spin-echo sequences, DRIVE can improve fluid–tissue contrast and enhance the conspicuity of subtle anatomical or pathological findings [33]. The three-dimensional nature of the acquisition also allows thin-section imaging and high-resolution multiplanar reconstructions, which are particularly useful for detecting small morphological abnormalities.

In clinical practice, 3D DRIVE offers several advantages in brain and spine imaging. The use of the driven equilibrium module may reduce acquisition time compared with conventional T2-weighted turbo spin-echo techniques, while maintaining high fluid signal. In addition, the sequence can reduce cerebrospinal fluid flow-related artifacts, improving visualization of structures surrounded by CSF, such as cranial nerves, spinal cord surfaces, cauda equina nerve roots, and intradural extramedullary lesions [32].

3D DRIVE shares some clinical applications with other heavily T2-weighted myelographic or cisternographic sequences, including balanced steady-state free precession techniques such as CISS and FIESTA. However, these sequences are based on different physical principles: CISS and FIESTA are gradient-echo-based balanced steady-state sequences, whereas DRIVE is based on a turbo spin-echo framework with a driven equilibrium recovery pulse. Despite these technical differences, all these sequences provide high contrast between CSF and adjacent neural or pathological structures and are therefore useful for the evaluation of fluid-containing spaces, cranial nerves, nerve roots, and small intradural lesions.

1.6.2 Applications in Brain and Spine Imaging

In neuroradiological practice, 3D DRIVE is widely used for high-resolution cisternographic imaging because of its ability to provide strong contrast between cerebrospinal fluid and

small neural or vascular structures. This makes it particularly useful for the evaluation of cranial nerves, the cerebellopontine angle, the internal auditory canal, and inner ear structures. Previous studies comparing 3D DRIVE with conventional three-dimensional T2-weighted turbo spin-echo sequences have shown slightly higher identification rates for several cranial nerve structures, including the Gasserian ganglion, the ophthalmic, maxillary, and mandibular divisions of the trigeminal nerve, and the cisternal segment of the abducens nerve. Overall image quality has also been reported to be superior with 3D DRIVE, particularly for fluid-containing structures such as the cochlea, vestibule, and semicircular canals [32]. 3D DRIVE has also been compared with three-dimensional balanced fast-field echo sequences for imaging of the internal auditory canal and inner ear, including acquisitions performed with sensitivity encoding techniques. In these settings, 3D DRIVE has been reported to provide high image quality and reduced artifacts, although both approaches can yield diagnostically adequate images [31,32]. In the internal auditory canal and cerebellopontine angle, 3D DRIVE may also help delineate the course of small vessels, such as the anterior inferior cerebellar artery and posterior inferior cerebellar artery, including vascular loops potentially related to neurovascular conflict syndromes [36].

Beyond cisternographic imaging, 3D DRIVE has been applied to the assessment of hypothalamic-pituitary disorders, including central precocious puberty, central diabetes insipidus, and hypopituitarism. In this context, its high spatial resolution may support the identification and measurement of pituitary stalk abnormalities and provide complementary information to post-contrast imaging [37].

The same imaging principles are relevant in spine MRI. Heavily T2-weighted myelographic sequences, including 3D DRIVE and balanced steady-state free precession techniques, are particularly effective for visualizing CSF-containing spaces and structures surrounded by CSF. By creating high contrast between hyperintense cerebrospinal fluid and hypointense nerve roots, membranes, or pathological deposits, these sequences can improve the assessment of the spinal canal, cauda equina, and dural cul-de-sac. In degenerative spine imaging, myelographic MRI sequences may help delineate extradural processes such as disc fragments, osteophytes, and spinal canal stenosis, providing a non-invasive alternative or complement to conventional CT myelography in selected clinical settings [38].

In pediatric neuro-oncology, their relevance is related to the detection of spinal leptomeningeal dissemination. Conventional post-contrast T1-weighted imaging remains a central component of spinal staging and follow-up, particularly for enhancing leptomeningeal disease. However, heavily T2-weighted myelographic sequences may increase the conspicuity of small intradural extramedullary deposits, especially when lesions are subtle, nodular, minimally enhancing, or non-enhancing. Their incorporation into spine MRI protocols may therefore improve diagnostic confidence, reduce interpretative uncertainty related to CSF pulsation artifacts, and support earlier detection of spinal metastatic spread in children with primary CNS tumors [37,38].

1.7 Study Rationale and Objectives

1.7.1 Gaps in Current Literature

Post-contrast T1-weighted imaging remains a key component of spinal MRI protocols for the detection of leptomeningeal dissemination in pediatric CNS tumors. However, increasing evidence suggests that heavily T2-weighted myelographic sequences, such as 3D DRIVE, CISS, and FIESTA, may provide additional diagnostic information by improving the visualization of small intradural lesions, nerve roots, cerebrospinal fluid spaces, and subtle abnormalities that may be obscured by flow-related artifacts.

Despite their potential diagnostic value, the implementation of high-resolution three-dimensional T2-weighted sequences in routine spinal MRI protocols remains variable across institutions. In many clinical settings, spine MRI is still largely based on conventional two-dimensional acquisitions, while 3D T2-weighted or myelographic sequences are used as complementary sequences rather than as systematically integrated components of the protocol. Current recommendations, including RAPNO guidelines, recognize the usefulness of high-resolution T2-weighted myelographic sequences for the assessment of leptomeningeal spread. Nevertheless, their incremental value over conventional post-contrast T1-weighted imaging, particularly for early, small, minimally enhancing, or non-enhancing spinal metastases, remains insufficiently defined in clinical practice.

This variability creates a relevant area for further investigation. A more systematic evaluation of 3D DRIVE may help clarify whether its routine incorporation into pediatric spine MRI protocols can improve early detection of spinal metastatic dissemination and increase diagnostic confidence, particularly in subtle or equivocal cases.

1.7.2 Aims of the Study

The present study aims to evaluate the added diagnostic value of the 3D DRIVE sequence for the detection of spinal metastases in pediatric patients with primary CNS tumors. In particular, the study focuses on the ability of 3D DRIVE to improve the visualization of subtle, small, nodular, minimally enhancing, or non-enhancing intradural lesions that may be difficult to identify on conventional post-contrast T1-weighted imaging alone.

Earlier and more confident detection of spinal metastatic dissemination may have relevant clinical implications, including more accurate staging, improved risk stratification, timely adaptation of therapeutic planning, definition of radiotherapy fields or focal boosts, and optimization of follow-up surveillance.

The primary objective of this study is therefore to compare 3D DRIVE with post-contrast T1-weighted imaging in the detection and characterization of spinal metastatic lesions. Secondary objectives include the evaluation of lesion morphology, anatomical distribution, involvement of the cauda equina and dural cul-de-sac, and the potential role of subtle CSF contour irregularities as early imaging findings.

2 Materials and Methods

2.1 Study Design and Population

This retrospective observational study was conducted at the IRCCS Istituto Giannina Gaslini through the review of clinical, radiological, and imaging data retrieved from the institutional Radiology Information System (RIS) and Picture Archiving and Communication System (PACS).

All patient data were handled in accordance with applicable data protection regulations, including Regulation (EU) 2016/679 — General Data Protection Regulation — and processed in compliance with the ethical principles of the Declaration of Helsinki.

2.1.1 Inclusion and Exclusion Criteria

Patients were eligible for inclusion if they were 18 years of age or younger at the time of diagnosis, had a primary CNS tumor, and were referred to the IRCCS Istituto Giannina Gaslini between January 2010 and September 2025. All patients underwent spinal MRI as part of staging or follow-up surveillance for leptomeningeal and spinal metastatic dissemination.

Cases were identified through the institutional clinical and radiological archives, including the Radiology Information System and Picture Archiving and Communication System, in collaboration with pediatric neuro-oncologists and neurosurgeons.

Inclusion criteria were: diagnosis of a primary CNS tumor; evidence of spinal leptomeningeal or drop metastases either at initial diagnosis or during the clinical course; availability of at least one preoperative or baseline spinal MRI examination including a sagittal 3D DRIVE sequence; and availability of corresponding post-contrast T1-weighted images for comparison.

Exclusion criteria were: absence of a preoperative or baseline 3D DRIVE sequence; availability only of early postoperative examinations potentially affected by blood-related

artifacts, hemosiderin deposits, or postoperative changes; severe motion artifacts; or insufficient image quality preventing reliable evaluation of metastatic disease.

A total of 29 patients met the inclusion criteria and were included in the final analysis.

2.2 MRI Acquisition Protocols

Spine MRI examinations were performed at the IRCCS Istituto Giannina Gaslini using either a 1.5T MRI scanner (Philips Intera/Achieva, Best, The Netherlands; installed in 2005) or a 3T MRI scanner (Philips Ingenia CX, Best, The Netherlands, installed in 2016). Spinal acquisitions were performed in the same imaging session as brain MRI, according to the institutional pediatric neuro-oncology protocol.

The spinal MRI protocol included post-contrast sagittal T1-weighted turbo spin-echo sequences and sagittal 3D DRIVE sequences. All acquisitions were performed using phased-array SENSE coils, with an 8-channel coil for the 1.5T system and a 32-channel coil for the 3-T system. For 1.5T examinations, sagittal post-contrast T1-weighted turbo spin-echo images were acquired with typical TR/TE values of approximately 450/6 ms, a flip angle of 90°, a slice thickness of 3 mm, and a field of view of approximately 250–280 mm, adjusted according to patient size. Sagittal 3D DRIVE images were acquired with typical TR/TE values of approximately 1500/150 ms, a slice thickness of 2 mm, and high in-plane spatial resolution, with a cranio-caudal field of view ranging from 400 to 520 mm depending on patient age and spinal coverage. For 3T examinations, sagittal post-contrast T1-weighted turbo spin-echo images were acquired with TR/TE values ranging from approximately 500–700/6 ms, a slice thickness of 3 mm, and a field of view of 450–500 mm. Sagittal 3D DRIVE images were acquired with TR/TE values of approximately 1000/230 ms, a slice thickness of 0.8–1 mm, and near-isotropic spatial resolution, with an average field of view of approximately 559 × 140 × 32 mm.

A standardized institutional protocol was used across patients, with technical adjustments according to scanner type, patient size, age, and the number of volumetric acquisition blocks required to obtain adequate spinal coverage. The protocol was designed to cover the

cervicothoracic and thoracolumbar spinal segments and, whenever possible, the conus medullaris, cauda equina, and dural cul-de-sac. In approximately two-thirds of baseline examinations, the sagittal 3D DRIVE field of view included the cauda equina and dural cul-de-sac, allowing assessment of potential caudal metastatic deposits. In the remaining baseline examinations, the cul-de-sac was not included because of limited acquisition coverage. Coverage of the dural cul-de-sac became more systematic in subsequent follow-up examinations. Therefore, cul-de-sac involvement was specifically evaluated only in examinations in which this region was included within the field of view.
Acquisition parameters were optimized to obtain diagnostic image quality and comparable spatial resolution across patients of different ages and body sizes.

2.3 Image Analysis and Classification

All spine MRI examinations were reviewed by two pediatric neuroradiologists, with 4 and 8 years of experience, respectively. The readers were blinded to the histological diagnosis at the time of image review. Image quality and sequence adequacy were first assessed, and examinations with severe motion artifacts or insufficient diagnostic quality were excluded from the analysis.

For each examination, the presence, visibility, and conspicuity of spinal metastatic lesions were assessed on the two main sequences: sagittal 3D DRIVE and post-contrast sagittal T1-weighted turbo spin-echo imaging. Findings were recorded using a categorical visibility score: 0 = no metastases visible; 1 = visible only on 3D DRIVE; 2 = visible only on post-contrast T1-weighted imaging; 3 = equally visible on both sequences; 4 = better depicted on 3D DRIVE than on post-contrast T1-weighted imaging; 5 = better depicted on post-contrast T1-weighted imaging than on 3D DRIVE.

The anatomical site of metastatic involvement was documented for each examination and categorized as spinal cord surface, cauda equina nerve roots, dural cul-de-sac, or combinations of these locations. Cul-de-sac involvement was evaluated only when this region was included within the field of view. Metastatic morphology was classified as linear, nodular, or mixed. Linear involvement was defined as smooth or plaque-like leptomeningeal thickening along the spinal cord surface or nerve roots, whereas nodular involvement was

defined as focal rounded or ovoid intradural deposits. Mixed morphology was assigned when both linear and nodular components were present in the same examination. An additional exploratory imaging finding, termed “laciniae”, was recorded when subtle thin protrusions, filaments, or irregularities of the cerebrospinal fluid contour were visible on 3D DRIVE images without a definite corresponding enhancing nodule on post-contrast T1-weighted imaging. These findings were analyzed descriptively as potential early morphological abnormalities preceding overt metastatic deposits.

Final metastatic status was established by consensus review, taking into account all available MRI examinations, longitudinal imaging evolution, topographic correspondence on follow-up studies, and multidisciplinary clinical-radiological assessment. The analysis was performed on a per-patient and per-examination basis, including baseline and up to five follow-up examinations per patient when available. Equivocal or discordant findings were jointly reviewed to reach a final consensus classification.

2.4 Statistical Analysis

Statistical analysis was performed using IBM SPSS Statistics software, version 26.0 (IBM Corp., Armonk, NY, USA). Continuous variables were assessed for normality using the Shapiro–Wilk test. Normally distributed variables were reported as mean ± standard deviation, whereas non-normally distributed variables were reported as median and interquartile range. Categorical variables were reported as frequencies and percentages. Descriptive statistics were used to summarize demographic data, tumor characteristics, MRI acquisition parameters, presence or absence of laciniae, lesion morphology, anatomical distribution of spinal metastases, and dural cul-de-sac involvement.

The diagnostic yield of 3D DRIVE and post-contrast T1-weighted imaging was compared using the McNemar test for paired categorical data. Comparisons were performed at baseline and at each available follow-up examination. A matched odds ratio was calculated to estimate whether metastatic lesions were more frequently detected or better depicted by 3D DRIVE compared with post-contrast T1-weighted imaging. Odds ratio values were interpreted as follows: OR = 1 indicated no difference between sequences; OR > 1 indicated

higher diagnostic yield for 3D DRIVE; and OR < 1 indicated higher diagnostic yield for post-contrast T1-weighted imaging. The association between metastatic morphology — linear, nodular, or mixed — and the sequence showing superior lesion conspicuity was assessed using Fisher's exact test. A Kaplan–Meier time-to-detection analysis was performed to evaluate the temporal distribution of metastatic lesion detection for each sequence. Differences between detection curves were compared using the log-rank Mantel–Cox test.

Given the retrospective design, the limited sample size, and the presence of repeated examinations in the same patients, statistical analyses were considered exploratory. Statistical significance was defined as a two-sided p-value ≤ 0.05.

3 Results

3.1 Baseline Characteristics and Tumor Grading

Patient characteristics are summarized in Table 1.

BASE DEMOGRAPHIC DATA		
Age (Years)		11.7 ± 7.4
Gender	F	18 (59%)
	M	11 (41%)
Tesla	1,5	5 (17%)
	3	24 (83%)
Grade	*I*	7 (24%)
	II	2 (8%)
	IV	20 (69%)
Surgery		28 (97%)

Table 1*: summary of subject characteristics.*

The mean age at diagnosis was 11.7 ± 7.4 years. The study population included 18 female patients (59%) and 11 male patients (41%). At baseline MRI, 5 patients (17%) were examined on a 1.5T scanner, whereas 24 patients (83%) were examined on a 3T scanner.

Most patients had high-grade tumors, with WHO grade 4 lesions observed in 20 cases (69%). Surgical procedures were performed in 28 patients (97%). The only patient who did not undergo surgery had a diffuse midline glioma diagnosed on the basis of clinical and radiological findings, as biopsy was considered unsafe.

3.2 Metastatic Distribution and Morphology over Follow-up

Imaging characteristics and evaluation parameters are summarized in Table 2.

	BASELINE	FU 1	FU 2	FU 3	FU 4	
Available Patients (#)	**29**	**29**	**25**	**19**	**11**	**6**
Time from baseline, months (Mdn; IQR)	n.a	5; 10	19; 27	29; 60	65; 54	102; 57
Sequence /Metastases*	**n (%)**	**n (%)**	**n (%)**	**n (%)**	**n (%)**	**n (%)**
0	18 (62%)	7 (24%)	6 (24%)	3 (19)	3 (27)	1 (17)
1	3 (11%)	8 (28%)	4 (16%)	4 (25)	4 (36)	0 (0)
2	2 (8%)	1 (3%)	2 (8%)	1 (6)	0 (0)	0 (0)
3	6 (22%)	13 (44%)	13 (52%)	11 (50)	4 (36)	5 (83)
4	4 (67%)	10 (77%)	9 (69%)	5 (46)	4 (100)	5 (100)
5	2 (33%)	3 (23%)	4 (31%)	6 (54)	0 (0)	0 (0)
MTX Morphology						
no	15 (52)	6 (21)	6 (24)	3 (16)	3 (27)	1 (17)
linear	1 (3)	1 (3)	2 (8)	1 (5)	0 (0)	0 (0)
nodular	7 (24)	13 (59)	13 (52)	12 (63)	8 (73)	2 (33)
linear + nodular	3 (10)	8 (28)	4 (16)	3 (16)	0 (0)	3 (50)
laciniae	3 (10)	n.a	n.a	n.a	n.a	n.a
Cul de Sac Acquisition**						
Yes	19 (66)	25 (86)	22 (88)	18 (95)	9 (82)	6 (100)
No	10 (34)	4 (14)	3 (12)	1 (5)	2 (18)	0 (0)
Location	**n=11**	**n=22**	**n=19**	**n=16**	**n=8**	**n=6**
Spinal cord surface	3 (27)	6 (27)	4 (21)	5 (31)	1 (12)	0 (0)
Caudal nerves roots	0 (0)	0 (0)	1 (5)	0 (0)	0 (0)	1 (20)
Cul de sac	1 (9)	1 (5)	1 (5)	2 (13)	0 (0)	0 (0)
Surface + caudal roots	3 (27)	5 (22)	3 (15)	3 (19)	2 (25)	1 (20)
Caudal roots + cul de sac	0 (0)	4(18)	1 (5)	1 (6)	2 (25)	0 (0)
Surface + cul de sac	2 (18)	2 (9)	3 (15)	1 (6)	1 (12)	2 (40)
All locations	2 (18)	4 (18)	6 (31)	4 (25)	2 (25)	1 (20)

***: 0= no metastases detected; 1= only with DRIVE; 2= only with T1WI; 3= detected equally on both; 4= DRIVE > T1; 5= DRIVE < T1 **: in 3D DRIVE*

***Table 2:** spinal metastases distribution among FU, including morphology, presence of laciniae, cul-de-sac acquisition, locations and visibility in 3D DRIVE and post-contrast T1WI*

At baseline, spinal metastases were identified in 11 of 29 patients (38%). Among patients with metastatic disease, nodular morphology was the most frequent pattern, observed in 7 of 11 cases (64%), followed by mixed linear-nodular morphology in 3 cases (27%) and purely linear morphology in 1 case (9%). Among lesions visible on both sequences, 3D DRIVE provided better lesion conspicuity than post-contrast T1-weighted imaging in 4 of 6 cases (67%), whereas post-contrast T1-weighted imaging was superior in 2 of 6 cases (33%). The dural cul-de-sac was included in the acquisition field of view in 19 of 29 baseline examinations (66%).

At the first follow-up, spinal metastases were present in 22 of 29 patients (76%). Nodular morphology remained the predominant pattern, observed in 13 of 22 metastatic cases (59%), followed by mixed linear-nodular morphology in 8 cases (36%) and purely linear morphology in 1 case (5%). Among cases in which lesions were visible on both sequences, 3D DRIVE showed greater conspicuity in 10 of 13 cases (77%), whereas post-contrast T1-weighted imaging was superior in 3 of 13 cases (23%). The dural cul-de-sac was included in the field of view in 25 patients (86%).

At the second follow-up, spinal metastases were observed in 19 of 25 patients (76%). Nodular morphology was present in 13 of 19 metastatic cases (68%), mixed morphology in 4 cases (21%), and linear morphology in 2 cases (11%). Among lesions visible on both sequences, 3D DRIVE provided greater conspicuity in 9 of 13 cases (69%), compared with post-contrast T1-weighted imaging in 4 of 13 cases (31%). The dural cul-de-sac was included in 22 examinations (88%).

At the third follow-up, metastases were evident in 16 of 19 patients (84%). Nodular morphology was again predominant, observed in 12 of 16 metastatic cases (75%), while mixed morphology was present in 3 cases (19%) and linear morphology in 1 case (6%). The dural cul-de-sac was included in 18 examinations (95%). Among lesions visible on both sequences, 3D DRIVE showed greater conspicuity in 5 of 11 cases (45%), whereas post-contrast T1-weighted imaging was superior in 6 of 11 cases (55%).

At the fourth follow-up, available in 11 patients, spinal metastases were observed in 8 cases (73%). All metastatic cases showed nodular morphology. Among lesions visible on both sequences, 3D DRIVE provided greater conspicuity in all evaluable cases (4/4; 100%). The dural cul-de-sac was included in 9 examinations (82%).

At the fifth follow-up, available in 6 patients, spinal metastases were present in 5 cases (83%). Mixed linear-nodular morphology was observed in 3 of 5 metastatic cases (60%), whereas purely nodular morphology was observed in 2 cases (40%). Among lesions visible on both sequences, 3D DRIVE provided greater conspicuity in all evaluable cases (5/5; 100%). The dural cul-de-sac was included in all examinations (6/6; 100%).

Overall, across available follow-up examinations, spinal metastases were frequently detected and were predominantly nodular or mixed in morphology. 3D DRIVE generally provided greater conspicuity than post-contrast T1-weighted imaging, particularly at early follow-up examinations and in later examinations with complete cul-de-sac coverage. Coverage of the dural cul-de-sac became progressively more systematic over time, reaching complete inclusion at the final follow-up.

3.3 Comparative Diagnostic Performance (Odds Ratio and McNemar test)

The trend of the odds ratio (OR) and corresponding McNemar test p-values at baseline and across follow-ups are illustrated in Figure 1:

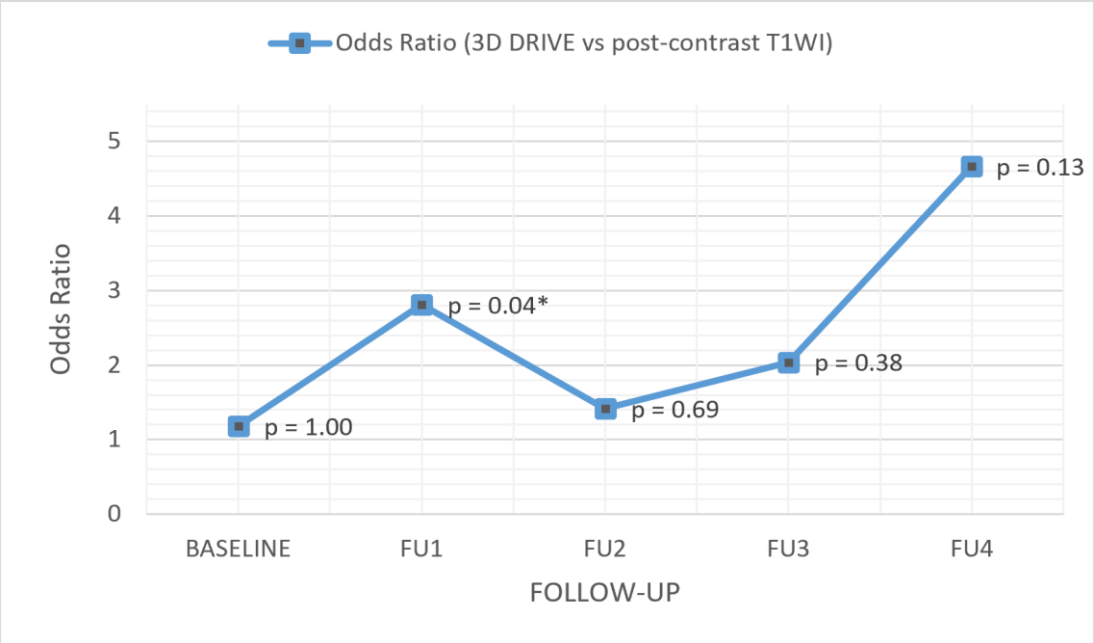

***:** $p < 0.05$ (statistical significance, McNemar test**)**

Figure 1: *Evolution of the Odds Ratio (3D DRIVE vs. post-contrast T1WI) across follow-up examinations. McNemar test p-values are shown for each follow-up time point.*

At baseline, no statistically significant difference was observed between 3D DRIVE and post-contrast T1-weighted imaging (OR = 1.18; p = 1.00), indicating no evidence of a sequence-related difference in metastatic lesion detection at initial assessment. At the first follow-up, 3D DRIVE showed a statistically significant advantage over post-contrast T1-weighted imaging, with a matched odds ratio of 2.81 and a McNemar test p-value of 0.04. This finding suggests a higher diagnostic yield of 3D DRIVE at early follow-up, particularly for subtle or small metastatic lesions.

In subsequent follow-up examinations, odds ratio values remained above 1, suggesting a trend favoring 3D DRIVE, although statistical significance was not reached: FU2, OR = 1.42, p = 0.69; FU3, OR = 2.04, p = 0.38; FU4, OR = 4.67, p = 0.13. These results should be interpreted with caution because of the progressively smaller number of available examinations and the exploratory nature of the analysis. The fifth follow-up was not included in the inferential analysis because of the limited sample size (n = 6), which did not allow a robust odds ratio estimation.

Overall, the comparative analysis demonstrated a significant advantage of 3D DRIVE at the first follow-up, with a non-significant trend favoring 3D DRIVE in later follow-up examinations. These findings support the potential added value of 3D DRIVE as a complementary sequence to post-contrast T1-weighted imaging, particularly in early metastatic surveillance.

3.4 Morphological Correlation and Fisher's Exact Test

The association between metastatic morphology (linear, nodular, laciniae, or combined) and the most effective MRI sequence for their detection was assessed using Fisher's exact test (Table 3).

Follow-up	**Fisher's exact test (p)**
Baseline	0,218
FU1	0,006
FU2	0,705
FU3	0,275
FU4	n.a
FU5	n.a

***Table 3**: association of morphology and MRI sequence (3D DRIVE vs post-contrast T1WI) across FU*

At the first follow-up, Fisher's exact test demonstrated a statistically significant association between metastatic morphology and the sequence providing superior lesion conspicuity ($p = 0.006$). In this analysis, nodular metastases were more often better depicted on 3D DRIVE,

whereas linear leptomeningeal involvement was more often better visualized on post-contrast T1-weighted imaging.

At later follow-up examinations, this association was no longer statistically significant (FU2: $p = 0.705$; FU3: $p = 0.275$). Given the limited number of observations at each follow-up, these results should be interpreted as exploratory.

3.5 Specialized Focus: The Cul-de-Sac Involvement

A dedicated analysis of dural cul-de-sac involvement was performed to assess the frequency and temporal distribution of caudal spinal metastases. For each follow-up examination, the number of patients with cul-de-sac involvement and the number of newly detected caudal metastatic deposits were recorded.

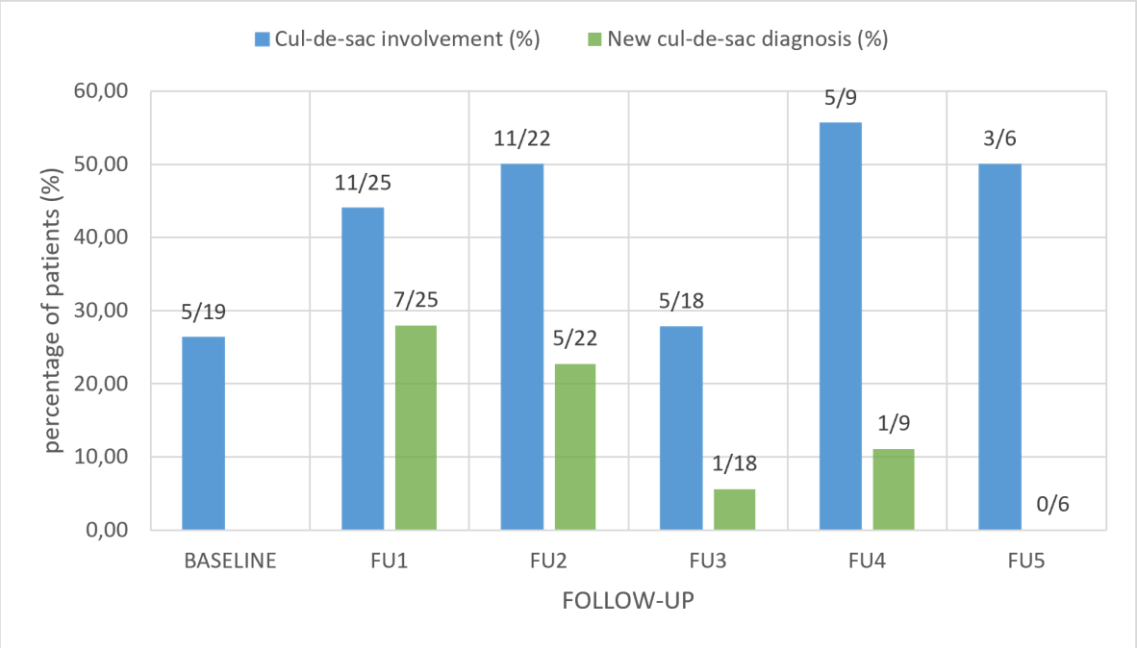

Figure 2: *patients with metastases localized in the cul-de-sac across follow-ups.*

The analysis of dural cul-de-sac involvement, shown in Figure 2, demonstrated that among examinations in which this region was included within the field of view, the prevalence of cul-de-sac metastases ranged from 26% at baseline (5/19 patients) to a maximum of 56% at

the fourth follow-up (5/9 patients). When only newly detected cul-de-sac involvement was considered, the proportion of new cases ranged from 6% to 28%, with the highest value observed at the first follow-up, where 7 new cases were identified among 25 patients with adequate cul-de-sac coverage.

Across all time points, caudal metastatic deposits were either visible only on 3D DRIVE or more clearly depicted on 3D DRIVE than on post-contrast T1-weighted imaging (Figure 3). In some cases, post-contrast T1-weighted images showed only nonspecific enhancement of the cauda equina nerve roots, which was insufficient for confident identification of focal metastatic deposits. Finally, the dural cul-de-sac was included in only 19 of 29 baseline examinations (66%). Coverage progressively increased during follow-up, reaching 86% at the first follow-up and more than 90% from the second follow-up onward.

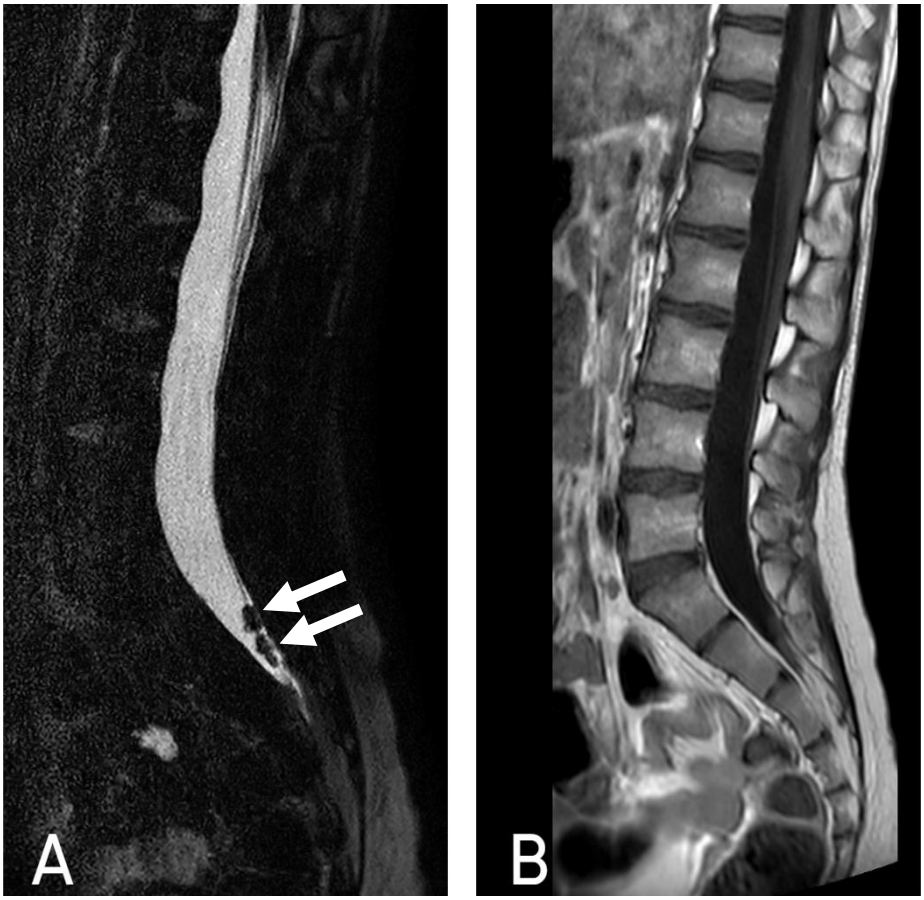

Figure 3: *example of cul-de-sac metastases visible in 3D DRIVE (arrwos, A) while not visible in post-contrast T1WI (B)*

3.6 Longitudinal Analysis and Early Detection (Kaplan–Meier Estimates)

To evaluate the temporal distribution of spinal metastasis detection across MRI sequences, a survival analysis was performed using the Kaplan–Meier method, comparing 3D DRIVE with post-contrast T1WI (Figure 4).

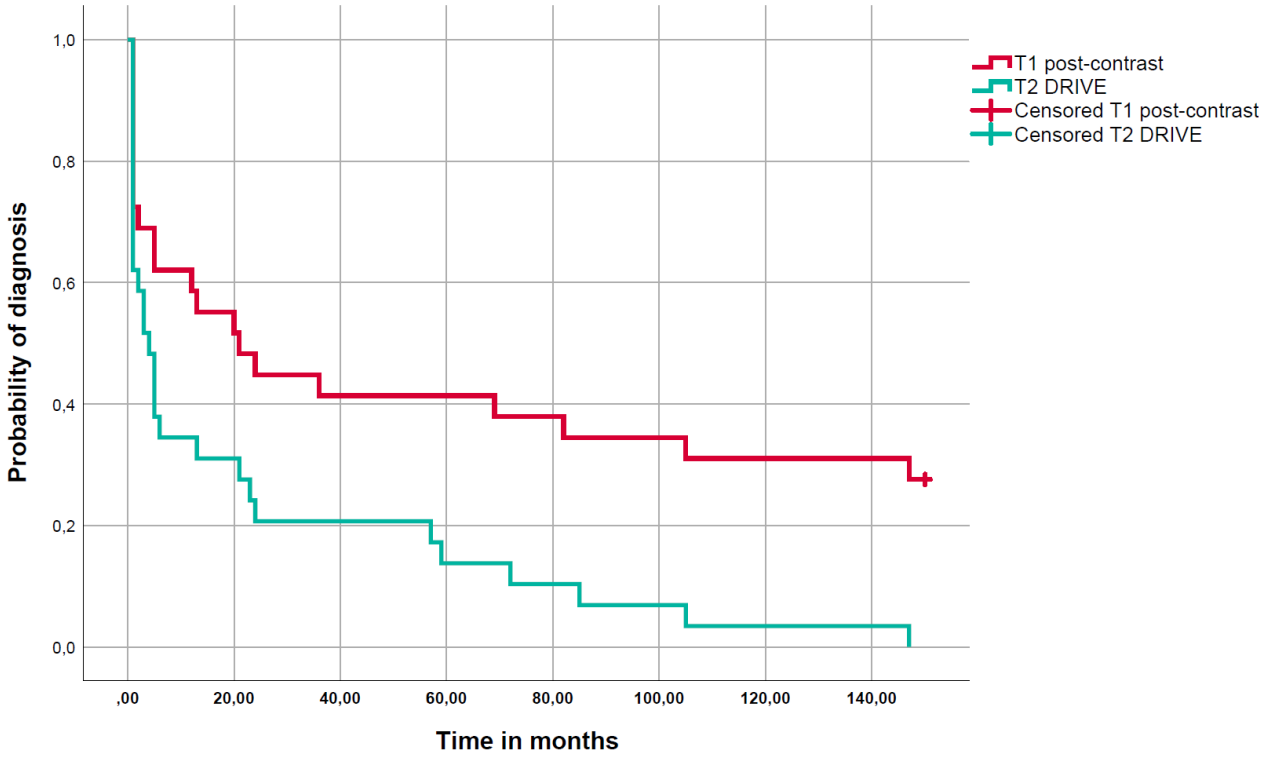

***Figure 4**: Kaplan-Meier curve for metastases' detection in T2 DRIVE and T1 post-contrast, compared using Log rank test.*

The Kaplan–Meier time-to-detection analysis showed earlier identification of spinal metastatic lesions on 3D DRIVE compared with post-contrast T1-weighted imaging. The estimated mean time to metastasis detection was 22.4 months for 3D DRIVE (95% CI: 8.8–36.0) and 60.3 months for post-contrast T1-weighted imaging (95% CI: 36.7–83.9).

Comparison of the detection curves using the log-rank Mantel–Cox test demonstrated a statistically significant difference between the two sequences ($p = 0.003$), supporting earlier

radiological detection with 3D DRIVE. This finding suggests that 3D DRIVE may provide added value in identifying spinal metastatic disease before it becomes clearly evident on post-contrast T1-weighted images.

3.7 The Predictive Role of "Laciniae": Descriptive Observations

A descriptive analysis was performed to assess the presence of “laciniae”, defined as subtle filiform protrusions or irregularities of the cerebrospinal fluid contour visible on 3D DRIVE images. These findings were recorded as exploratory imaging observations and were not considered definite metastatic lesions at baseline.

Laciniae were identified at baseline in three patients (3/29; 10.3%). All three patients subsequently developed overt spinal metastatic lesions in the same anatomical regions where the initial laciniae had been observed. Although no formal statistical analysis could be performed because of the small number of cases, this finding suggests a possible topographic relationship between early CSF contour irregularities and subsequent metastatic deposits.

It should also be noted that additional potentially positive cases may have been excluded from this descriptive analysis because their first available 3D DRIVE examinations were obtained in the postoperative setting. In these cases, blood-related artifacts, hemosiderin deposits, or postoperative changes could have interfered with the reliable assessment of subtle CSF contour abnormalities.

In the case illustrated in Figure 5, the baseline 3D DRIVE image (A) shows subtle hyperintense laciniae along the dorsal CSF contour, without a corresponding abnormality on the post-contrast T1-weighted image (B). At the 5-month follow-up, nodular metastatic deposits became visible in the same region on 3D DRIVE (C) and appeared as punctate enhancing lesions on post-contrast T1-weighted imaging (D), supporting a topographic correspondence with the initial DRIVE findings.

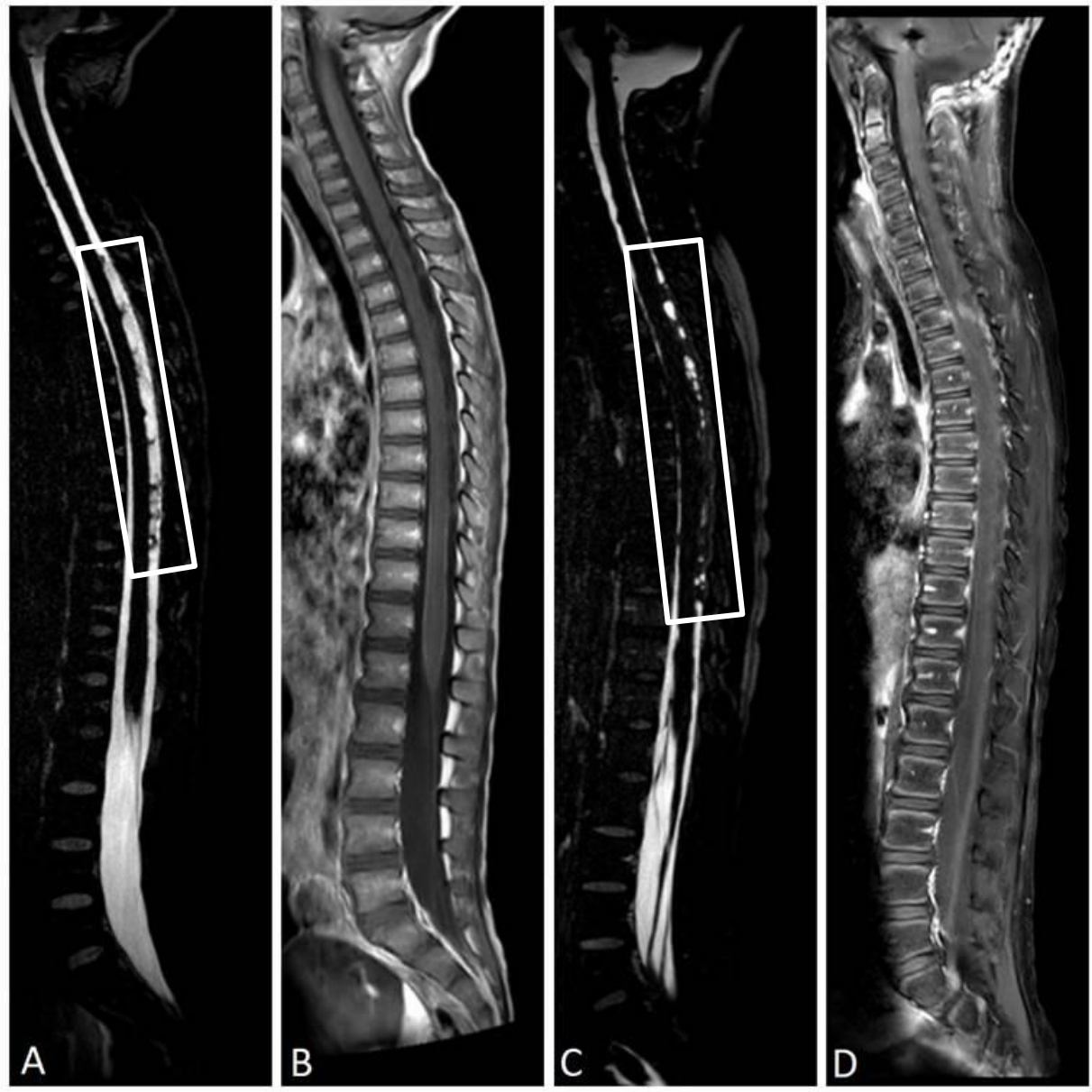

Figure 5*: example of laciniae's evolution over time. (A) 3D DRIVE at baseline shows subtle laciniae along CSF contour (box). (B) post-contrast T1WI at baseline where the same findings are not visible. (C) Follow-up examination with 3D DRIVE with hypointense nodular lesions (box). (D) Follow-up examination with post-contrast T1 showing nodular enhancement compatible with leptomeningeal metastases*

Similar findings were observed in the other two cases. In both patients, subtle laciniae identified on baseline 3D DRIVE images were followed by the development of nodular metastatic deposits in corresponding anatomical regions. Taken together, these three cases suggest a possible spatial relationship between early CSF contour irregularities on 3D DRIVE and subsequent overt leptomeningeal metastatic lesions.

4 Discussion

At present, spinal assessment in pediatric patients with primary CNS tumors relies primarily on post-contrast T1-weighted imaging and sagittal T2-weighted sequences, as recommended by current RAPNO guidelines [20]. However, conventional sequences may be limited in the detection of small, subtle, or non-enhancing metastatic deposits, particularly during the early stages of leptomeningeal dissemination [39,40].

Recent literature has emphasized that the diagnostic yield of spinal MRI for leptomeningeal dissemination depends strongly on technical acquisition quality. Key factors include thin-section imaging, absence of interslice gaps, complete coverage of the spinal canal including the cauda equina and dural cul-de-sac, and integration of high-CSF-contrast sequences such as DRIVE, CISS, FIESTA, or SPACE [39,41,42]. These sequences may improve visualization of subtle abnormalities of the leptomeningeal or CSF contour that are not clearly detectable on conventional post-contrast T1-weighted imaging.

In this context, the present study evaluated the added diagnostic value of 3D DRIVE within pediatric spine MRI protocols for patients with primary CNS tumors, with particular attention to its role in the early detection and characterization of spinal leptomeningeal metastatic spread.

4.1 Performance of Myelographic Sequences in Pediatric Spine Imaging

3D DRIVE, similarly to other high-CSF-contrast myelographic sequences such as CISS and FIESTA, provides high spatial resolution, strong contrast between cerebrospinal fluid and adjacent soft-tissue structures, and reduced sensitivity to CSF flow-related artifacts compared with conventional T2-weighted spin-echo sequences [39,43]. These properties make it particularly suitable for the evaluation of small anatomical or pathological structures surrounded by CSF. As reported by Godano et al. [35], 3D DRIVE demonstrated high anatomical resolution in the assessment of subtle CSF-adjacent structures, such as the pituitary stalk, even without contrast administration, owing to its favorable CSF–tissue

contrast. Similarly, Roser et al. [41] showed that CISS sequences, which provide a myelographic effect comparable to that of 3D DRIVE, offer high subarachnoid contrast and reduced signal loss related to CSF flow compared with conventional T2-weighted spin-echo imaging. This resulted in improved assessment of subtle arachnoid webs and spinal cord cavitations.

In the present study, 3D DRIVE showed similar advantages in the evaluation of spinal leptomeningeal metastatic disease. The sequence provided high CSF contrast and improved conspicuity of small intradural nodular metastases, while maintaining acquisition times compatible with pediatric MRI protocols. This technical advantage was associated with a higher diagnostic yield compared with post-contrast T1-weighted imaging, particularly during early follow-up examinations.

4.2 DRIVE vs. T1 Post-Contrast: Sensitivity in Early Stages

Several studies have reported that the integration of heavily T2-weighted myelographic sequences with post-contrast T1-weighted imaging may improve the detection of spinal leptomeningeal disease. For example, Kralik et al. [40] showed that combining post-contrast 3D T1-weighted VIBE with 3D T2-weighted SPACE improved the detection of subarachnoid disease and increased inter-reader reliability.

In the present study, McNemar analysis demonstrated a statistically significant difference between 3D DRIVE and post-contrast T1-weighted imaging at the first follow-up, with a matched odds ratio of 2.81 in favor of 3D DRIVE. This finding suggests that, at early follow-up, 3D DRIVE provides a higher diagnostic yield than post-contrast T1-weighted imaging for the detection of spinal metastatic lesions. In subsequent follow-up examinations, odds ratio values fluctuated and did not reach statistical significance. This variability is likely influenced by the limited sample size and the progressively smaller number of available examinations over time. A further possible explanation is that, as metastatic deposits become larger or more conspicuous during disease progression, they may also become more readily detectable on post-contrast T1-weighted imaging, reducing the relative difference between the two sequences.

These findings are consistent with previous reports suggesting that the added value of high-CSF-contrast myelographic sequences is particularly relevant in early disease stages, when metastatic deposits may be small, subtle, minimally enhancing, or non-enhancing, and surrounded by cerebrospinal fluid [37].

4.3 Morphological Insights: Identifying Non-Enhancing Nodules

The morphology of leptomeningeal metastases represents an important diagnostic parameter. Butch et al. [36] reported that high-CSF-contrast bSSFP sequences improve the visualization of small intradural nodular deposits, whereas post-contrast T1-weighted imaging remains essential for detecting linear leptomeningeal enhancement, often described as a “sugar-coating” pattern. In the present study, morphological analysis supported the complementary role of the two sequences. 3D DRIVE showed greater conspicuity for nodular metastatic deposits, particularly during early follow-up examinations, whereas post-contrast T1-weighted imaging remained particularly useful for identifying linear leptomeningeal enhancement.

These findings suggest that 3D DRIVE may be especially valuable in the early detection of small nodular deposits, including lesions that are subtle, minimally enhancing, or not yet clearly visible on post-contrast T1-weighted images. Conversely, post-contrast T1-weighted imaging remains crucial for the assessment of diffuse or linear leptomeningeal involvement, where contrast enhancement reflects disruption of the blood–CSF barrier or vascularized leptomeningeal disease. This interpretation is consistent with previous observations suggesting that leptomeningeal dissemination may show different imaging patterns over time, ranging from small nodular or non-enhancing deposits to more diffuse linear enhancement along the leptomeningeal surfaces [43].

Overall, these data support the concept that 3D DRIVE and post-contrast T1-weighted imaging should be considered complementary rather than alternative sequences. 3D DRIVE may improve the detection and characterization of small nodular deposits, while post-

contrast T1-weighted imaging remains indispensable for evaluating enhancing linear or diffuse leptomeningeal disease.

4.4 Clinical Relevance of the Cul-de-Sac

Current RAPNO recommendations emphasize the importance of complete spinal MRI coverage, including the cauda equina and dural cul-de-sac, in pediatric CNS tumors at risk of leptomeningeal dissemination [20]. The lumbar cul-de-sac represents a clinically relevant region because CSF circulation and gravity-dependent pathways may favor the accumulation of tumor cells in caudal subarachnoid spaces, making the cauda equina roots and dural cul-de-sac potential sites of early metastatic deposition [40,44].

The findings of the present study support this pattern. Among examinations in which the dural cul-de-sac was included within the field of view, cul-de-sac involvement was observed in 26% of patients at baseline, increased to 44% at the first follow-up, and reached 50% at the second follow-up. Although later time points included fewer patients, the prevalence of cul-de-sac involvement remained high, reaching 56% at the fourth follow-up. In nearly all patients with metastatic deposits in this region, lesions were either visible only on 3D DRIVE or more clearly depicted on 3D DRIVE than on post-contrast T1-weighted imaging. By contrast, post-contrast T1-weighted images sometimes showed only nonspecific enhancement of the cauda equina nerve roots, which was not sufficient for confident identification of focal metastatic deposits. These results are consistent with previous reports by Roser et al. [41] and Godano et al. [35], which highlighted the value of high-CSF-contrast sequences for depicting subtle abnormalities and small structures surrounded by cerebrospinal fluid.

Overall, the present findings suggest that the dural cul-de-sac is not only a frequent site of spinal metastatic dissemination but may also represent an early site of detectable disease. Systematic inclusion of this region in sagittal 3D DRIVE acquisitions requires only a limited increase in acquisition time and may provide substantial diagnostic benefit. Accurate identification of cul-de-sac involvement may influence treatment planning, including

adaptation of radiation fields, extension of irradiation to the thecal sac when appropriate, or delivery of focal radiation boosts to sites of metastatic involvement.

4.5 Temporal correlation and Kaplan Meier analysis

Kaplan–Meier time-to-detection analysis showed that spinal metastatic lesions became radiologically evident earlier on 3D DRIVE than on post-contrast T1-weighted imaging. The estimated mean time to detection was 22.4 months for 3D DRIVE and 60.3 months for post-contrast T1-weighted imaging, with a statistically significant difference between the two detection curves according to the log-rank test ($p = 0.003$). This finding supports the added diagnostic value of 3D DRIVE during the early stages of leptomeningeal dissemination.

This longitudinal result distinguishes the present study from previous investigations, which have predominantly relied on cross-sectional comparisons, and highlights the importance of serial imaging assessment in the surveillance of pediatric patients with primary CNS tumors [39,40].

These findings are consistent with the observations of Harreld and Patay [39], who reported that high-CSF-contrast sequences, including 3D bSSFP and post-contrast T2-FLAIR, may increase the sensitivity of MRI for leptomeningeal metastatic disease. In a similar manner, the time-to-detection curve in the present study suggests that 3D DRIVE may reveal spinal metastatic deposits before they become clearly visible on post-contrast T1-weighted imaging. This concept is also comparable to the observations reported by Morana et al. [44], in which diffusion-weighted imaging allowed earlier identification of cerebral tumor relapse before clear abnormalities were evident on post-contrast T1-weighted imaging. Analogously, 3D DRIVE may play a complementary role in spine MRI by improving early detection of subtle leptomeningeal deposits and potentially supporting earlier therapeutic adjustment. Finally, the review by Kuah et al. [38] emphasized that heavily T2-weighted myelographic sequences provide excellent differentiation of intradural structures because of their high CSF contrast and reduced susceptibility to flow-related artifacts. This reinforces the rationale for incorporating 3D DRIVE into spinal MRI protocols for pediatric CNS tumors at risk of leptomeningeal dissemination.

4.6 Additional observations: Laciniae

An original exploratory observation emerging from this study concerns the presence of subtle irregularities of the cerebrospinal fluid contour, referred to as “laciniae”, which were identified on 3D DRIVE images in three patients (10.3%). In all three cases, follow-up imaging demonstrated the subsequent development of overt nodular metastatic deposits in the same anatomical regions, suggesting a possible topographic relationship between these early CSF contour abnormalities and later metastatic involvement.

Previous studies by Roser et al. [43] and Buch et al. [39] described subtle leptomeningeal or subarachnoid abnormalities detectable with high-resolution, high-CSF-contrast sequences, interpreting them as possible adhesions, arachnoid changes, or small subarachnoid deposits. In the present study, the observed laciniae may represent an earlier morphological stage preceding the appearance of definite nodular metastases. This interpretation remains exploratory but raises the hypothesis that subtle CSF contour irregularities on 3D DRIVE could act as potential pre-nodular imaging signs of leptomeningeal dissemination.

The clinical relevance of this observation lies in the possibility that early recognition of such findings may prompt closer imaging surveillance and may help identify patients at risk of developing overt spinal metastatic disease. In selected cases, the detection of additional nodular lesions or early spinal dissemination could influence therapeutic planning, including the choice between focal treatment strategies and broader craniospinal approaches. However, larger prospective studies with standardized imaging protocols and longer follow-up are required to validate the significance of laciniae and to determine whether they have true predictive value.

4.7 Study Limitations and Potential Imaging Pitfalls

Like all retrospective studies, this analysis has several limitations that should be considered when interpreting the results.

The first limitation is the relatively small sample size. This limited the statistical power of the study and required the integration of inferential analyses with descriptive observations,

particularly for subgroup analyses, late follow-up examinations, cul-de-sac involvement, and the exploratory assessment of laciniae. Therefore, some findings should be considered hypothesis-generating rather than definitive.

A second limitation is the heterogeneity of imaging follow-up. Examinations were performed over a long time interval, from 2009 to 2025, with variable intervals between follow-up studies and using different MRI systems, including both 1.5T and 3T scanners. These factors may have introduced variability in image quality, spatial resolution, signal-to-noise ratio, and sensitivity for small metastatic deposits.

Several imaging pitfalls should also be considered. Hemosiderin deposits, postoperative blood products, or surgical-related changes may appear as nonspecific hypointense foci on 3D DRIVE images and could potentially mimic small intradural metastatic lesions. To reduce this bias, patients for whom only early postoperative examinations were available were excluded from the study.

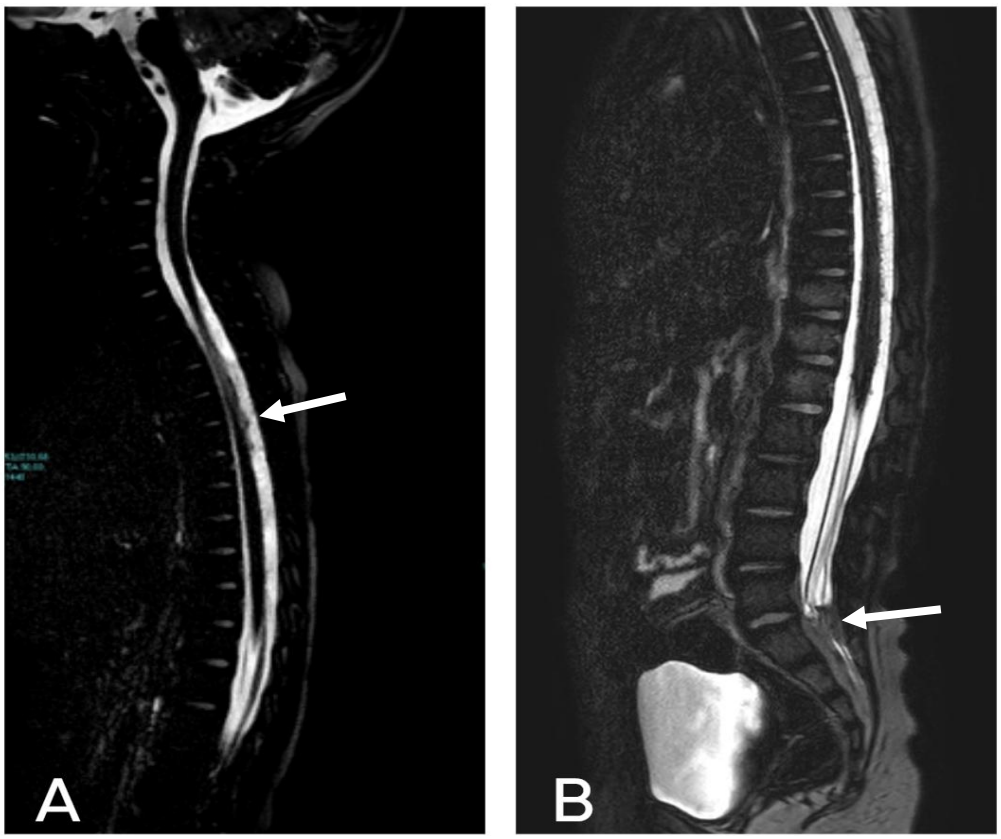

Figure 6*: areas of hypointensity in 3D DRIVE localized in the dorsal region (arrow, A) and cul-de-sac (arrow, B) caused by hemosiderin deposits after surgery, not correlated with metastatic foci.*

Another potential imaging pitfall is represented by focal dural or leptomeningeal irregularities, which may mimic small metastatic deposits. In the representative case shown in Figure 6, the finding remained stable on all subsequent examinations and did not show contrast enhancement, making metastatic involvement unlikely.

Such findings should be interpreted cautiously, taking into account morphology, enhancement pattern, clinical context, temporal evolution, and comparison with previous examinations. Longitudinal follow-up is essential to differentiate true metastatic deposits from benign, postoperative, or nonspecific dural abnormalities (Figure 7).

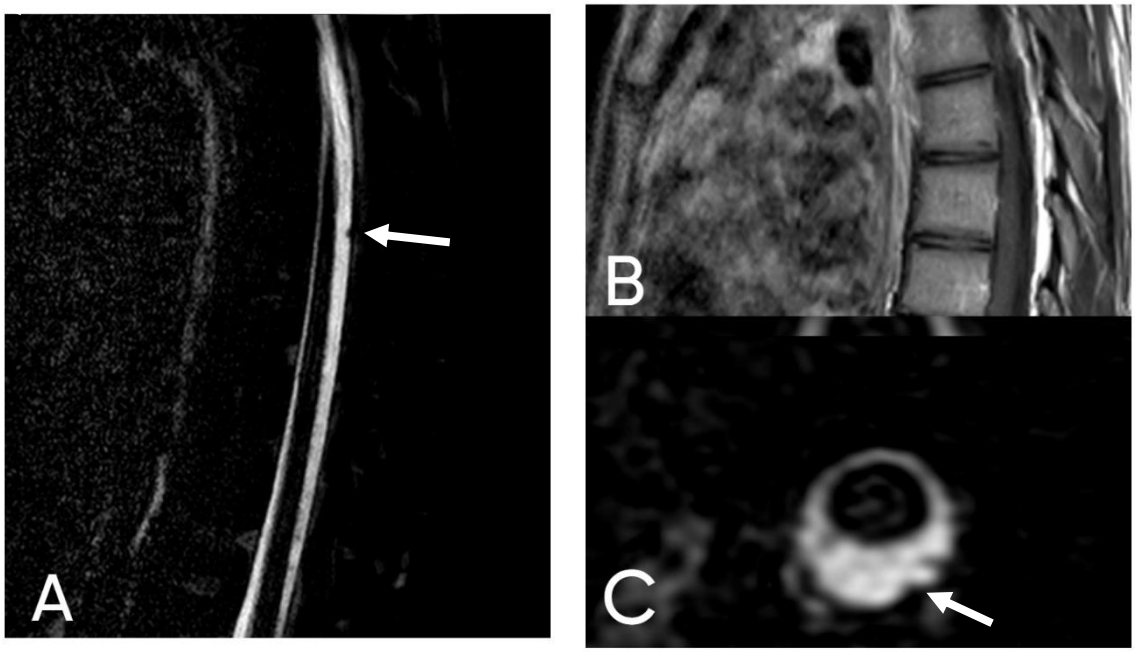

Figure 7: *dural irregularity showed in 3D DRIVE on the sagittal (arrow, A) and axial (arrow, C) planes, without contrast enhancement (B).*

In another patient, shown in Figure 8, an apparent metastatic focus on MRI was subsequently attributed to a displaced surgical clip, as confirmed by CT. This case emphasizes the value of multimodality correlation in equivocal postoperative findings.

Careful integration of MRI, CT, surgical history, and prior imaging is therefore essential to avoid false-positive interpretation and prevent inappropriate therapeutic decisions, such as unnecessary focal radiation boost planning.

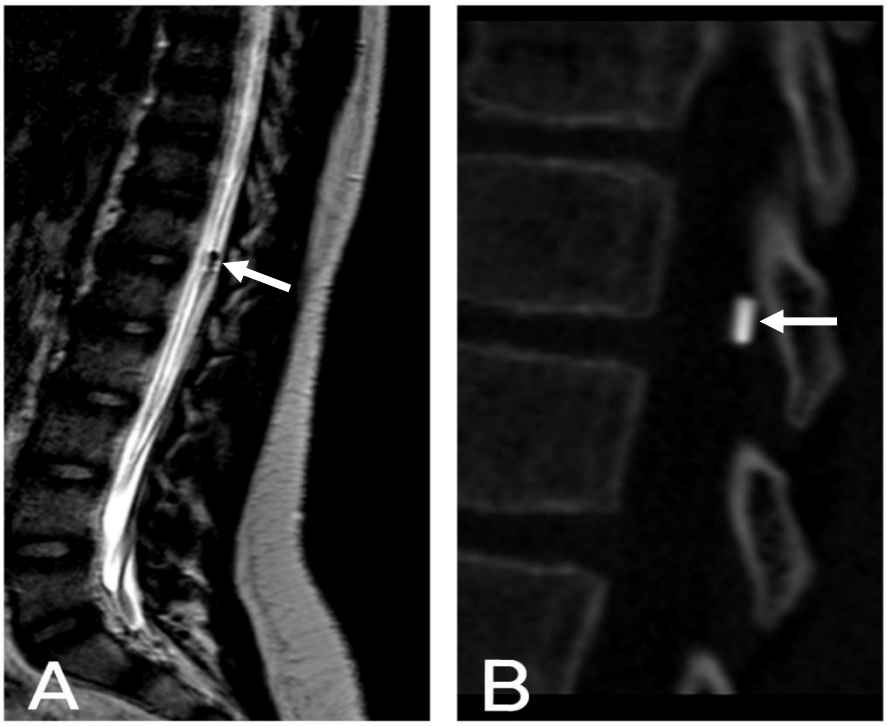

Figure 8: *example case of false positive; an apparent nodular lesion visible in the thoracolumbar region in 3D DRIVE (arrow, A) was revealed to be a surgical clip by CT scan (arrow, B).*

Lastly, CSF flow-related artifacts are a relevant technical pitfall in spine MRI, as they may occasionally simulate small intradural metastatic deposits. Although usually identifiable by experienced readers, these artifacts can be misleading at first assessment. In the representative case shown in Figure 9, a focal CSF signal irregularity in the dorsolumbar region initially raised concern for a small intradural lesion. Its stability on follow-up examinations, together with the absence of associated enhancement or morphological progression, supported an artifactual rather than metastatic origin.

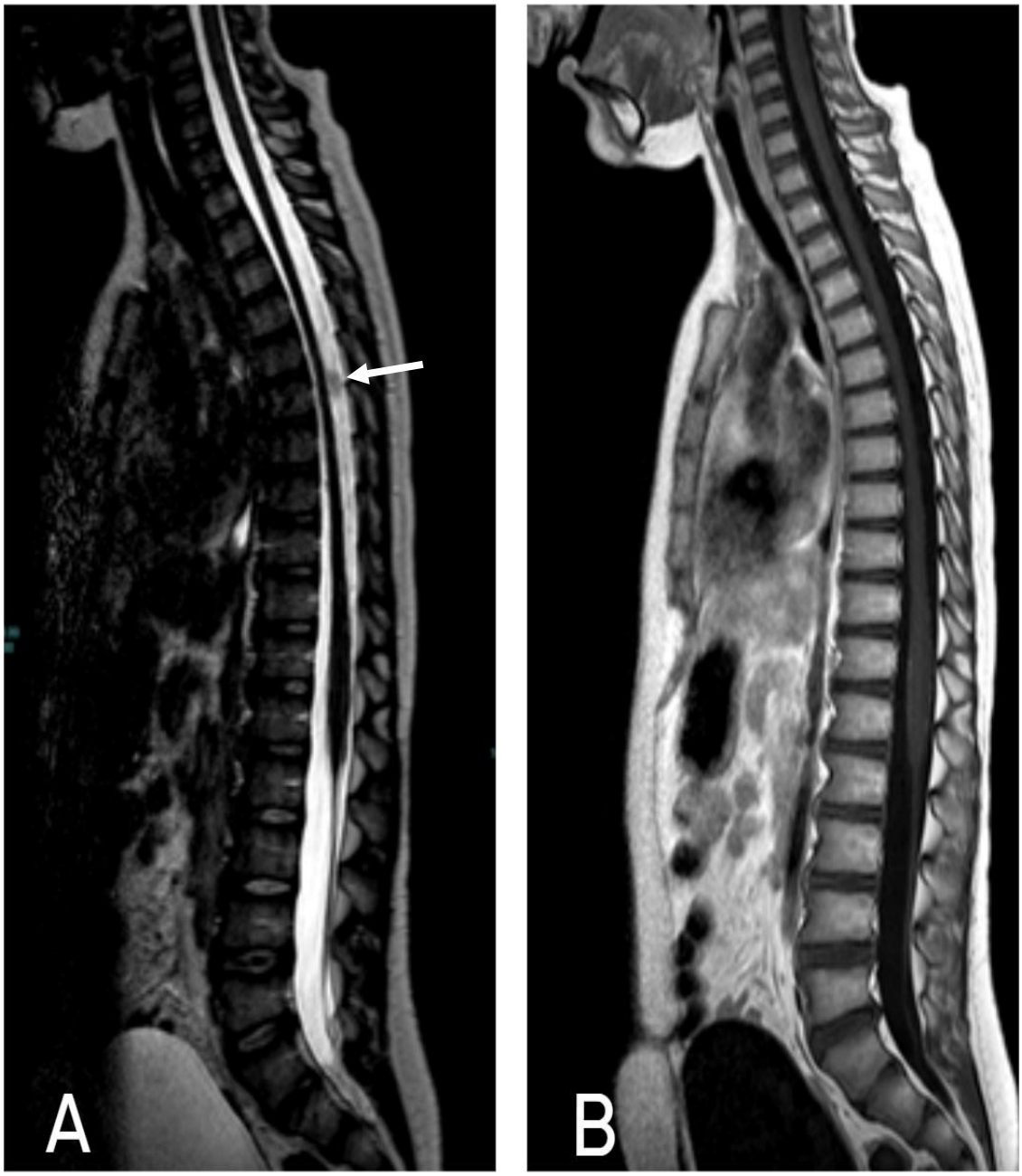

Figure 9: *artifact caused by CSF flow; linear area of hypointensity in 3D DRIVE (arrow, A) without an equivalent finding in post-contrast T1WI (B).*

5 Conclusions

3D DRIVE may represent a valuable complementary sequence to post-contrast T1-weighted imaging for the assessment of spinal leptomeningeal metastases in pediatric patients with primary CNS tumors. The most relevant advantage emerged during early follow-up, where 3D DRIVE showed improved conspicuity of small, nodular, minimally enhancing, or non-enhancing intradural lesions. This may have important clinical implications, as earlier detection of spinal metastatic dissemination can contribute to more accurate staging, risk stratification, therapeutic planning, and follow-up surveillance.

Particular attention should be paid to the cauda equina and dural cul-de-sac, which represent frequent sites of caudal “drop” metastases. In this study, systematic inclusion of this region in sagittal 3D DRIVE acquisitions increased the ability to detect small caudal metastatic deposits that could be overlooked on conventional post-contrast T1-weighted imaging alone.

The observation of subtle CSF contour irregularities, referred to as “laciniae”, represents an exploratory finding. Although identified in a limited number of cases, these abnormalities showed spatial correspondence with subsequent nodular metastatic deposits, suggesting that they may represent early pre-nodular imaging signs of leptomeningeal dissemination. This hypothesis requires validation in larger prospective cohorts.

Overall, the present findings support the incorporation of 3D DRIVE as a complementary high-resolution myelographic sequence in pediatric spine MRI protocols for patients at risk of leptomeningeal metastatic spread. Future multicenter studies with larger populations, standardized acquisition protocols, and longer longitudinal follow-up are needed to confirm these results and to define the role of 3D DRIVE in international imaging recommendations.

Bibliography

1. Louis DN, Perry A, Wesseling P, Brat DJ, Cree IA, Figarella-Branger D, et al. The 2021 WHO Classification of Tumors of the Central Nervous System: a summary. Neuro Oncol. 2021 Aug 2;23(8):1231–51. doi:10.1093/neuonc/noab106 PubMed PMID: 34185076; PubMed Central PMCID: PMC8328013.

2. Halfpenny AM, Wood MD. Review of the Recent Changes in the WHO Classification for Pediatric Brain and Spinal Cord Tumors. Pediatr Neurosurg. 2023;58(5):337–55. doi:10.1159/000528957 PubMed PMID: 36617415; PubMed Central PMCID: PMC10664345.

3. Osborn AG, Louis DN, Poussaint TY, Linscott LL, Salzman KL. The 2021 World Health Organization Classification of Tumors of the Central Nervous System: What Neuroradiologists Need to Know. AJNR Am J Neuroradiol. 2022 Jul;43(7):928–37. doi:10.3174/ajnr.A7462 PubMed PMID: 35710121; PubMed Central PMCID: PMC9262075.

4. Agarwal A, Bathla G, Soni N, Desai A, Ajmera P, Rao D, et al. Newly Recognized Genetic Tumor Syndromes of the CNS in the 5th WHO Classification: Imaging Overview with Genetic Updates. AJNR Am J Neuroradiol. 2024 Feb 7;45(2):128–38. doi:10.3174/ajnr.A8039 PubMed PMID: 37945522; PubMed Central PMCID: PMC11285983.

5. Hawkins C, Aldape K, Capper D, von Deimling A, Giannini C, Gilbert MR, et al. cIMPACT-NOW update 10: Recommendations for defining new types for central nervous system tumor classification. Brain Pathol. 2025 Nov;35(6):e70018. doi:10.1111/bpa.70018 PubMed PMID: 40420507; PubMed Central PMCID: PMC12488253.

6. Lamba N, Wen PY, Aizer AA. Epidemiology of brain metastases and leptomeningeal disease. Neuro Oncol. 2021 Sep 1;23(9):1447–56. doi:10.1093/neuonc/noab101 PubMed PMID: 33908612; PubMed Central PMCID: PMC8408881.

7. Ostrom, al. CBTRUS Statistical Report: Pediatric Brain Tumor Foundation Childhood and Adolescent Primary Brain and Other Central Nervous System Tumors Diagnosed in the United States in 2014–2018. Neuro-oncology. 2022;24(S3):iii1–38. doi:https://doi.org/10.1093/neuonc/noac161

8. Ostrom, Q. T., Francis, S. S., & Barnholtz-Sloan, J. S. (2021). Epidemiology of Brain and Other CNS Tumors. Current Neurology and Neuroscience Reports, 21(12). https://doi.org/10.1007/s11910-021-01152-9.

9. Wu J, Heidelberg R, Gajjar A. Wu J, Heidelberg RE, Gajjar A. Adolescents and Young Adults With Cancer: CNS Tumors. J Clin Oncol. 2024 Feb 20;42(6):686-695. doi: 10.1200/JCO.23.01747. Epub 2023 Dec 8. PMID: 38064656; PMCID: PMC11550794. J Clin Oncol. 2024 Feb 20;42(6):686–95. doi:10.1200/JCO.23.01747

10. Ostrom QT, Adel Fahmideh M, Cote DJ, Muskens IS, Schraw JM, Scheurer ME, et al. Risk factors for childhood and adult primary brain tumors. Neuro Oncol. 2019 Nov 4;21(11):1357–75. doi:10.1093/neuonc/noz123 PubMed PMID: 31301133; PubMed Central PMCID: PMC6827837.

11. Kleinerman RA. Cancer risks following diagnostic and therapeutic radiation exposure in children. Pediatr Radiol. 2006 Sep;36 Suppl 2(Suppl 2):121–5. doi:10.1007/s00247-006-0191-5 PubMed PMID: 16862418; PubMed Central PMCID: PMC2663653.

12. Hansford JR, Das A, McGee RB, Nakano Y, Brzezinski J, Scollon SR, et al. Update on Cancer Predisposition Syndromes and Surveillance Guidelines for Childhood Brain Tumors. Clin Cancer Res. 2024 Jun 3;30(11):2342–50. doi:10.1158/1078-0432.CCR-23-4033 PubMed PMID: 38573059; PubMed Central PMCID: PMC11147702.

13. Chen DY, Chen CC, Crawford JR, Wang SG. Tumor-related epilepsy: epidemiology, pathogenesis and management. J Neurooncol. 2018 Aug;139(1):13–21. doi:10.1007/s11060-018-2862-0 PubMed PMID: 29797181.

14. Wilne S, Collier J, Kennedy C, Koller K, Grundy R, Walker D. Presentation of childhood CNS tumours: a systematic review and meta-analysis. Lancet Oncol. 2007 Aug;8(8):685–95. doi:10.1016/S1470-2045(07)70207-3 PubMed PMID: 17644483.

15. Cagney DN, Martin AM, Catalano PJ, Redig AJ, Lin NU, Lee EQ, et al. Incidence and prognosis of patients with brain metastases at diagnosis of systemic malignancy: a population-based study. Neuro Oncol. 2017 Oct 19;19(11):1511–21. doi:10.1093/neuonc/nox077 PubMed PMID: 28444227; PubMed Central PMCID: PMC5737512.

16. Suki D, Hatiboglu MA, Patel AJ, Weinberg JS, Groves MD, Mahajan A, et al. Comparative risk of leptomeningeal dissemination of cancer after surgery or stereotactic radiosurgery for a single supratentorial solid tumor metastasis. Neurosurgery. 2009 Apr;64(4):664–74; discussion 674-676. doi:10.1227/01.NEU.0000341535.53720.3E PubMed PMID: 19197219.

17. Le Rhun E, Weller M, Brandsma D, Van den Bent M, de Azambuja E, Henriksson R, et al. EANO-ESMO Clinical Practice Guidelines for diagnosis, treatment and follow-up of patients with leptomeningeal metastasis from solid tumours. Ann Oncol. 2017 Jul 1;28(suppl_4):iv84–99. doi:10.1093/annonc/mdx221 PubMed PMID: 28881917.

18. Cooney TM, Cohen KJ, Guimaraes CV, Dhall G, Leach J, Massimino M, et al. Response assessment in diffuse intrinsic pontine glioma: recommendations from the Response Assessment in Pediatric Neuro-Oncology (RAPNO) working group. Lancet Oncol. 2020 Jun;21(6):e330–6. doi:10.1016/S1470-2045(20)30166-2 PubMed PMID: 32502459.

19. Warren KE, Vezina G, Poussaint TY, Warmuth-Metz M, Chamberlain MC, Packer RJ, et al. Response assessment in medulloblastoma and leptomeningeal seeding tumors: recommendations from the Response Assessment in Pediatric Neuro-Oncology committee. Neuro Oncol. 2018 Jan 10;20(1):13–23. doi:10.1093/neuonc/nox087 PubMed PMID: 28449033; PubMed Central PMCID: PMC5761545.

20. Geraldo AF, Maldonado F, Severino M, Mankad K, Dahmoush H, Soares B, et al. Response assessment in pediatric neurooncology (RAPNO) criteria revisited: a practical navigation guide for neuroradiologists. Neuroradiology. 2024 Dec;66(12):2117–42. doi:10.1007/s00234-024-03493-x PubMed PMID: 39446196.

21. Erker C, Tamrazi B, Poussaint TY, Mueller S, Mata-Mbemba D, Franceschi E, et al. Response assessment in paediatric high-grade glioma: recommendations from the

Response Assessment in Pediatric Neuro-Oncology (RAPNO) working group. Lancet Oncol. 2020 Jun;21(6):e317–29. doi:10.1016/S1470-2045(20)30173-X PubMed PMID: 32502458.

22. Silva AHD, Aquilina K. Surgical approaches in pediatric neuro-oncology. Cancer Metastasis Rev. 2019 Dec;38(4):723–47. doi:10.1007/s10555-019-09832-2 PubMed PMID: 31863234.

23. Lanier JC, Abrams AN. Posterior fossa syndrome: Review of the behavioral and emotional aspects in pediatric cancer patients. Cancer. 2017 Feb 15;123(4):551–9. doi:10.1002/cncr.30238 PubMed PMID: 27787875.

24. Jackson K, Packer RJ. Recent Advances in Pediatric Medulloblastoma. Curr Neurol Neurosci Rep. 2023 Dec;23(12):841–8. doi:10.1007/s11910-023-01316-9 PubMed PMID: 37943476; PubMed Central PMCID: PMC10724301.

25. Malik JR, Podany AT, Khan P, Shaffer CL, Siddiqui JA, Baranowska-Kortylewicz J, et al. Chemotherapy in pediatric brain tumor and the challenge of the blood-brain barrier. Cancer Med. 2023 Dec;12(23):21075–96. doi:10.1002/cam4.6647 PubMed PMID: 37997517; PubMed Central PMCID: PMC10726873.

26. Damodharan S, Puccetti D. Pediatric Central Nervous System Tumor Overview and Emerging Treatment Considerations. Brain Sci. 2023 Jul 21;13(7). doi:10.3390/brainsci13071106 PubMed PMID: 37509034; PubMed Central PMCID: PMC10377074.

27. Bou Dargham T, Winter SF, Batich K, Gehring K, Parsons MW, Dietrich J, et al. Neurocognitive outcomes in patients with brain metastases: a systematic review. Lancet Oncol. 2025 Dec;26(12):e671–82. doi:10.1016/S1470-2045(25)00525-X PubMed PMID: 41308688.

28. Michalski JM, Janss AJ, Vezina LG, Smith KS, Billups CA, Burger PC, et al. Children's Oncology Group Phase III Trial of Reduced-Dose and Reduced-Volume Radiotherapy With Chemotherapy for Newly Diagnosed Average-Risk Medulloblastoma. J Clin

Oncol. 2021 Aug 20;39(24):2685–97. doi:10.1200/JCO.20.02730 PubMed PMID: 34110925; PubMed Central PMCID: PMC8376317.

29. Oh J, Patel S, Schlosser MP, Arifin AJ, Oliveira C, Charpentier AM, et al. Pediatric CNS Radiation Oncology: Recent Developments and Novel Techniques. Curr Oncol. 2025 Mar 20;32(3):180. doi:10.3390/curroncol32030180 PubMed PMID: 40136384; PubMed Central PMCID: PMC11941344.

30. Becker ED, Feretti JA, Farrar TC. Driven Equilibrium Fourier Transform Spectroscopy. A New Method for Nuclear Magnetic Resonance Signal Enhancement. J Am Chem Soc. 1969 Dec 1;91(27):7784–5. doi:10.1021/ja50001a068

31. Serša I. Comparison of driven equilibrium and standard spin-echo sequence in MR microscopy: Analysis of signal dependence on RF pulse imperfection and diffusion. J Magn Reson. 2024 Feb;359:107624. doi:10.1016/j.jmr.2024.107624 PubMed PMID: 38241847.

32. Ciftci E, Anik Y, Arslan A, Akansel G, Sarisoy T, Demirci A. Driven equilibrium (drive) MR imaging of the cranial nerves V-VIII: comparison with the T2-weighted 3D TSE sequence. Eur J Radiol. 2004 Sep;51(3):234–40. doi:10.1016/j.ejrad.2003.10.019 PubMed PMID: 15294330.

33. Hargreaves BA, Gold GE, Lang PK, Conolly SM, Pauly JM, Bergman G, et al. MR imaging of articular cartilage using driven equilibrium. Magn Reson Med. 1999 Oct;42(4):695–703. doi:10.1002/(sici)1522-2594(199910)42:4<695::aid-mrm11>3.0.co;2-z PubMed PMID: 10502758.

34. Jung NY, Moon WJ, Lee MH, Chung EC. Magnetic resonance cisternography: comparison between 3-dimensional driven equilibrium with sensitivity encoding and 3-dimensional balanced fast-field echo sequences with sensitivity encoding. J Comput Assist Tomogr. 2007;31(4):588–91. doi:10.1097/rct.0b013e31809861fb PubMed PMID: 17882037.

35. Byun JS, Kim HJ, Yim YJ, Kim ST, Jeon P, Kim KH, et al. MR imaging of the internal auditory canal and inner ear at 3T: comparison between 3D driven equilibrium and 3D

balanced fast field echo sequences. Korean J Radiol. 2008;9(3):212–8. doi:10.3348/kjr.2008.9.3.212 PubMed PMID: 18525223; PubMed Central PMCID: PMC2627251.

36. Kazawa N, Togashi K, Ito J. The anatomical classification of AICA/PICA branching and configurations in the cerebellopontine angle area on 3D-drive thin slice T2WI MRI. Clin Imaging. 2013;37(5):865–70. doi:10.1016/j.clinimag.2011.11.021 PubMed PMID: 23751264.

37. Godano E, Morana G, Di Iorgi N, Pistorio A, Allegri AEM, Napoli F, et al. Role of MRI T2-DRIVE in the assessment of pituitary stalk abnormalities without gadolinium in pituitary diseases. Eur J Endocrinol. 2018 Jun;178(6):613–22. doi:10.1530/EJE-18-0094 PubMed PMID: 29650689.

38. Melhem ER, Itoh R, Folkers PJ. Cervical spine: three-dimensional fast spin-echo MR imaging--improved recovery of longitudinal magnetization with driven equilibrium pulse. Radiology. 2001 Jan;218(1):283–8. doi:10.1148/radiology.218.1.r01ja38283 PubMed PMID: 11152816.

39. Buch K, Caruso P, Ebb D, Rincon S. Balanced Steady-State Free Precession Sequence (CISS/FIESTA/3D Driven Equilibrium Radiofrequency Reset Pulse) Increases the Diagnostic Yield for Spinal Drop Metastases in Children with Brain Tumors. AJNR Am J Neuroradiol. 2018 Jul;39(7):1355–61. doi:10.3174/ajnr.A5645 PubMed PMID: 29773567; PubMed Central PMCID: PMC7655452.

40. Kralik SF, O'Neill DP, Kamer AP, Rodriguez E, Ho CY. Radiological diagnosis of drop metastases from paediatric brain tumours using combination of 2D and 3D MRI sequences. Clin Radiol. 2017 Oct;72(10):902.e13-902.e19. doi:10.1016/j.crad.2017.04.016 PubMed PMID: 28545686.

41. Kuah T, Vellayappan BA, Makmur A, Nair S, Song J, Tan JH, et al. State-of-the-Art Imaging Techniques in Metastatic Spinal Cord Compression. Cancers (Basel). 2022 Jul 5;14(13):3289. doi:10.3390/cancers14133289 PubMed PMID: 35805059; PubMed Central PMCID: PMC9265325.

42. Harreld JH, Khan A, Angel J, Han Y, Li Y, Gajjar A, et al. MRI sequences and interslice gap influence leptomeningeal metastasis detection in children with brain tumors. Neuroradiology. 2022 Jul;64(7):1447–56. doi:10.1007/s00234-022-02928-7 PubMed PMID: 35344053.

43. Roser F, Ebner FH, Danz S, Riether F, Ritz R, Dietz K, et al. Three-dimensional constructive interference in steady-state magnetic resonance imaging in syringomyelia: advantages over conventional imaging. J Neurosurg Spine. 2008 May;8(5):429–35. doi:10.3171/SPI/2008/8/5/429 PubMed PMID: 18447688.

44. Morana G, Alves CA, Tortora D, Severino M, Nozza P, Cama A, et al. Added value of diffusion weighted imaging in pediatric central nervous system embryonal tumors surveillance. Oncotarget. 2017 Sep 1;8(36):60401–13. doi:10.18632/oncotarget.19553 PubMed PMID: 28947980; PubMed Central PMCID: PMC5601148.